Naunyn-Schmiedeberg's Archives of Pharmacology
https://doi.org/10.1007/s00210-025-04627-5

RESEARCH

Inhibition of junctional protein disruption by 2,4,6-trihydroxy-3-geranyl acetophenone in lipopolysaccharide-induced endothelial hyperpermeability via GEF-H1/RhoA/ROCK pathway

Yee Han Chan[1] · Kong Yen Liew[1] · Kamal Rullah[2] · Hanis Hazeera Harith[1] · Ji Wei Tan[3] · Daud Ahmad Israf[1] · Khozirah Shaari[4,5] · Mexmollen Marcus[6] · Chau Ling Tham[1]

Received: 22 May 2025 / Accepted: 5 September 2025

Abstract

2,4,6-Trihydroxy-3-geranyl acetophenone (tHGA) is a bioactive phloroglucinol compound found in the leaves of *Melicope pteleifolia* (Champ. ex Benth.) T.G.Hartley. Our previous study has proven that tHGA exhibited significant in vitro barrier protective effects against lipopolysaccharide (LPS) induction, mainly by inhibiting endothelial hyperpermeability via attenuation of F-actin cytoskeletal rearrangement, as F-actin cytoskeleton is anchored to junctional proteins such as zonula occluden (ZO)-1, occludin, and vascular endothelial-cadherin (VE-cadherin), and they play collaborative roles in the preservation of endothelial integrity. Therefore, the effects of tHGA on these junctional proteins were further investigated, followed by the dissection of signalling pathways mediated by tHGA in suppressing LPS-induced junctional protein disruption during endothelial hyperpermeability. HUVECs were pretreated with tHGA prior to LPS induction. TEER, immunofluorescence staining, Western Blotting, and RT-qPCR were performed to examine the effects of tHGA on junctional proteins in terms of their integrity, localization, protein expression, and gene expression, respectively. Proinflammatory signalling molecules including MLC, NF-κB p65, p38 MAPK, ERK MAPK, and JNK MAPK were assessed to unravel the underlying signalling pathways, followed by molecular docking on human ROCK1 to predict the molecular target of tHGA. tHGA profoundly preserved junctional integrity by inhibiting both delocalization and downregulation of ZO-1, occludin, and VE-cadherin, via inactivation of MLC, NF-κB p65, p38 MAPK, and ERK MAPK, which are mainly diverged from GEF-H1/RhoA/ROCK pathway. ROCK1 was predicted as the molecular target of tHGA. tHGA should be developed as a potential therapeutic remedy for prevention and/or treatment of permeability-related disorders.

Keywords 2,4,6-Trihydroxy-3-geranyl acetophenone (tHGA) · *Melicope pteleifolia* (Champ. ex Benth.) T.G.Hartley. · Lipopolysaccharide (LPS) · Endothelial hyperpermeability · Junctional protein · Signalling pathway

Introduction

In vascular vessels, endothelial cells are interconnected by junctional protein complexes which are categorized into tight junctions (TJs), adherens junctions (AJs), and gap junctions (GJs) (Komarova et al. 2017). TJs include transmembrane proteins, namely occludin and claudin, as well as a cytoplasmic scaffolding protein, namely zonula occluden (ZO) (Vermette et al. 2018). On the other hand, AJs are composed of VE-cadherin and adhesion molecules, namely p120, α-catenin, and β-catenin (Garrett et al. 2017). Junctional proteins are highly intermingled with the F-actin cytoskeleton to maintain endothelial barrier integrity for the regulation of tissue-fluid homeostasis, particularly endothelial permeability. Under normal physiological conditions, endothelial permeability is preserved at the basal level and gradually increased in response to inflammatory stimuli such as lipopolysaccharide (LPS) to allow the migration of immune cells to the sites of injury (Claesson-Welsh et al. 2020).

LPS is a pathogen-associated molecular pattern (PAMP) found in the outer membrane of Gram-negative bacteria (Sullivan et al. 2011). During local or systemic engagement, LPS actively binds to host's pathogen recognition receptor, namely Toll-like receptor-4 (TLR-4) (Li et al. 2017), and triggers a series of proinflammatory signalling pathways including GEF-H1/RhoA/ROCK, nuclear factor

Extended author information available on the last page of the article

Published online: 16 October 2025

kappa-light-chain-enhancer of activated B cells (NF-κB), and mitogen-activated protein kinase (MAPK) pathways. These activations result in impaired vascular integrity and endothelial hyperpermeability as a consequence of compromised junctional protein complexes (Guo et al. 2012; Cho et al. 2014). Remarkably, the activation of proinflammatory signalling pathways could provoke the overproduction of proinflammatory cytokines and chemokines, which further exacerbates interstitial fluid leakage in an unrestricted manner (Dolmatova et al. 2021). These overwhelming vascular leakage and inflammatory responses will lead to endothelial dysfunction, multiple organ failure, and septic shock, ultimately causing death (Hu et al. 2015).

To date, numerous therapies have been approved and widely used in the current clinical settings for the treatment and/or management of endothelial hyperpermeability–related disorders. The most common one is undoubtedly glucocorticoids such as dexamethasone, triamcinolone acetanide, and hydrocortisone. Apart from their high potency and long-acting effects, glucocorticoids have been widely shown to reduce cytokine- and vascular endothelial growth factor (VEGF)–induced endothelial hyperpermeability, as well as improve blood–brain barrier integrity (van der Wijk et al. 2019). However, long-term usages of glucocorticoids could lead to numerous adverse side effects such as hypertension, osteoporosis, immunosuppression, and metabolic disturbance (Oray et al. 2016). Another approved therapy is synthetic somatostatin analogs (SSAs) such as octreoride and lanreotide. They have shown significant anti-inflammatory effects, reducing endothelial hyperpermeability, inflammation and ROS generation in various models (Fakir et al. 2024). As a Food and Drug Administration (FDA)–approved drug for neuroendocrine tumors, octreotide has been potential in alleviating LPS-induced endothelial injury by enhancing endothelial barrier function via the activation of activating transcription factor (ATF) 6 (Fakir and Barabutis 2024). However, they bring numerous side effects such as gastrointestinal disturbance, gallbladder contraction, and decreased hormone and enzyme secretion (Gomes-Porras et al. 2020). Besides that, one of the approved therapies is ranibizumab, a VEGF inhibitor which was proven effective for retinal diseases (Lowe et al. 2007). Although ranibizumab targets VEGF which plays a significant role in vascular permeability and angiogenesis, it requires high cost and possesses side effects such as myocardial infarction and ischemic stroke due to its anti-angiogenic action (Evoy & Abel 2013). Given these limitations, there is a clear need to discover and develop novel agents that are effective, selective, and safe in preserving endothelial barrier integrity. Moreover, natural product–derived compounds and bioactive phytochemicals are gaining interest due to their multi-targeted actions and favorable safety profiles, offering potential alternatives for treating endothelial dysfunction in inflammatory conditions (Pereira-Leite et al. 2017).

The compound of interest in our present study, 2,4,6-trihydroxy-3-geranyl acetophenone (tHGA), is a phloroglucinol compound found in the leaves of *Melicope pteleifolia* (Champ. ex Benth.) T.G.Hartley, a medicinal plant vernacularly known as *tenggek burung* (Fig. 1) (Karim et al. 2011). Our previous study demonstrated that tHGA protected endothelial cells against LPS induction via suppression of vascular inflammation and endothelial hyperpermeability. Interestingly, the suppressive effect of tHGA on vascular inflammation was solely contributed by the reduced adhesion and transmigration of monocytes across the activated endothelial barrier, through the alleviation of cell adhesion molecules (CAMs) and prostaglandin E_2 (PGE_2) production, but not the suppression of monocyte chemoattractant protein (MCP)−1 expression. The same study has also proven that the abrogation of LPS-induced endothelial hyperpermeability was partially attributed to the inhibitory effect exerted by tHGA on F-actin cytoskeletal rearrangement (Chong et al. 2016). These findings collectively suggested that the mode of action of tHGA may be due to its direct action on endothelium's structural changes rather than its ability to modulate the secretion of proinflammatory mediators. Given that F-actin cytoskeleton is connected to TJs and AJs, and these structures play collaborative roles in preserving endothelial integrity (Claesson-Welsh et al. 2020), the present study aimed to determine the effects of tHGA on junctional proteins and dissect the underlying signalling pathways.

Materials and methods

Chemicals, reagents, kits, and antibodies

EndoGro LS complete medium kit, trypsin-ethylenediamine tetraacetic acid (EDTA), polyvinylidene fluoride (PVDF) membrane, and bicinchoninic acid (BCA) protein assay kit were purchased from Merck Millipore (Massachusetts, USA). Phosphate-buffered saline (PBS) tablets, Tris, and sodium dodecyl sulfate (SDS) were purchased

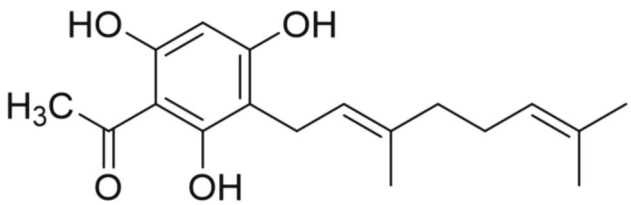

Fig. 1 Chemical structure of 2,4,6-trihydroxy-3-geranyl acetophenone (tHGA). Adopted from (Ismail et al. 2012)

from Amresco Life Science (Texas, USA). Dextran from *Leuconostoc* spp., LPS derived from *Escherichia coli* strain O111:B4, dexamethasone, sodium chloride (NaCl), paraformaldehyde, polyethylene glycol (PEG) 300, sodium deoxycholate, ammonium persulfate (APS), hydrochloric acid (HCl), Triton-X 100, and Tween-20 were purchased from Sigma-Aldrich (Missouri, USA). Prolong Gold antifade mounting reagent, and nuclear and cytoplasmic protein extraction reagents were purchased from Thermo Fisher Scientific (Massachusetts, USA). Glycine and bovine serum albumin (BSA) were purchased from Biobasic (Ontario, Canada). Absolute ethanol and methanol were purchased from Fisher Chemical (Massachusetts, USA). Protease inhibitor cocktail, 40% acrylamide, sodium azide, 6 × Laemmli's loading buffer, and RNase quiet were purchased from Nacalai Tesque (Kyoto, Japan). BLUeye prestained protein ladder was purchased from GeneDirex (USA). Tetramethylethylenediamine (TEMED) was purchased from HiMedia Laboratories (Mumbai, India). WesternBright Sirius enhanced chemiluminescence (ECL) and FlashBlot transfer buffer were purchased from Advansta Inc (California, USA). FavorPrep blood/cultured cell total ribonucleic acid (RNA) mini kit was purchased from Favorgen (Ping Tung, Taiwan). cDNA synthesis kit was purchased from Biotechnology Rabbit (Berlin, Germany). QuantiNova SYBR green PCR kit was purchased from Qiagen (Hilden, Germany). Forward and reverse primers of ZO-1, occludin, VE-cadherin, and glyceraldehyde-3-phosphate dehydrogenase (GAPDH) were purchased from Integrated DNA Technologies (Coralville, Lowa). ZO-1 (D6L1E) rabbit monoclonal antibody (#13,663), VE-cadherin (D87F2) XP rabbit monoclonal antibody (#2500), myosin light chain 2 rabbit monoclonal antibody (#3672), phospho-myosin light chain 2 (Ser19) rabbit monoclonal antibody (#3671), NF-κB p65 (D14E12) XP rabbit monoclonal antibody (#8242), p38 MAPK antibody (#9212), phospho-p38 MAPK (Thr180/Tyr182) rabbit monoclonal antibody (#9211), p44/42 ERK 1/2 MAPK rabbit monoclonal antibody (#9102), phosho-p44/42 ERK 1/2 MAPK (Thr202/Tyr204) (#9101), SAPK/JNK rabbit monoclonal antibody (#9252), phosho-SAPK/JNK (Thr183/Tyr185) rabbit monoclonal antibody (#9251), lamin A/C (4C11) mouse monoclonal antibody (#4777), horseradish peroxidase (HRP)-linked anti-rabbit IgG secondary antibody (#7074), Alexa Fluor 488-conjugated anti-rabbit IgG (#4412), and rabbit (DA1E) mAb IgG XP isotype control (#3900) were purchased from Cell Signaling Technology (Massachusetts, USA). Occludin rabbit monoclonal antibodies (#ab216327) and (#701,161) were purchased from Abcam (Cambridge, UK) and Invitrogen (Massachusetts, USA), respectively. HRP-linked beta-actin mouse monoclonal antibody (#sc-47778 HRP) was purchased from Santa Cruz Biotechnology (Texas, USA).

Synthesis and reconstitution of tHGA

tHGA was synthesized according to previously described methods (Ismail et al. 2012). For reconstitution, tHGA was dissolved in 100% DMSO to obtain a 20-mM stock solution which was later diluted with EndoGRO LS compete medium to obtain the respective working concentrations (Chong et al. 2016). In the present study, tHGA with concentrations of 1.25, 5, and 20 μM were tested as these concentrations were proven to be non-cytotoxic to human umbilical vein endothelial cells (HUVECs) (Chong et al. 2016).

Primary cell culture

HUVECs were purchased from Millipore Sigma (previously known as Merck Millipore), USA. The cells were cultured according to the manufacturer's protocols. Briefly, the cells were grown in T25 culture flasks containing EndoGRO LS complete medium and maintained at 37 °C in a 5% CO_2-humified incubator. Upon 80–90% confluency, the cells were subcultured or seeded at the density of 2×10^5 cells/mL. Only HUVECs between passages 1 to 5 were used (Chong et al. 2016).

Transendothelial electrical resistance (TEER) assay

HUVECs were seeded into 24-well transwell inserts (1.0-μm pore size) and cultured for 24 h. Once the cells reached 80–90% confluency, they were pretreated with tHGA (1.25, 5, and 20 μM) or dexamethasone (10 μM) for 6 h, followed by 24 h of LPS induction (1 μg/mL) as previously reported (Chong et al. 2016). In this study, 1 μg/mL LPS was used for induction as this concentration was not toxic to the cells and able to cause significant changes (compared to normal condition) on the parameters tested in the HUVEC model of our previous study. Similarly, the concentrations of tHGA (1.25, 5, and 20 μM) and dexamethasone (10 μM) were chosen because these concentrations were reported to be non-toxic to HUVECs and able to exerted significant inhibitory effects on the changes induced by LPS in the same model of our previous study (Chong et al. 2016).

To avoid possible osmolarity change that could influences endothelial hyperpermeability, respective osmolarity-matched molecules with similar molecular weights were included as osmolarity controls for transendothelial electrical resistance (TEER) assay. Specifically, polyethylene glycol (PEG) 300 with molecular weight of 300 g/mol was used as the osmolarity control for tHGA (304 g/mol). Although LPS is inherently heterogeneous in structure and the exact determination of its molecular weight is infeasible, its molecular weight was noted to be approximately 10 to 20 kDa. Therefore, dextran with similar molecular weight was used as the osmolarity control for LPS. The treatment

concentrations and conditions applied to PEG300 and dextran osmolarity control groups were exactly the same with LPS and tHGA control groups, respectively. TEER assay was then conducted according to previously described protocols with modifications (Wu et al. 2020). On the day of measurement, STX2 or "chopstick" electrode pairs were sterilized with 70% ethanol and dipped into 0.15 M sodium chloride for equilibration prior to measurement. The resistance values ($\Omega\ cm^2$) were taken after 24 h of LPS induction by using an epithelial volt/ohm meter (EVOM) (World Precision Instruments, USA). Inserts without cells were used as the blank. The resistance value of each well was corrected by subtracting it with the resistance value of the blank to obtain the normalized TEER value. The results were expressed as the percentage of control (Wu et al. 2020).

To avoid measurement biasness, the experimental groups were randomly assigned to the wells across the plate. The plate layout was documented in a separate record, and no treatment labels were indicated directly on the plate. All resistance values were measured objectively using consistent and standardized equipment settings. Data were analyzed under blinded condition using coded sample identifiers. By applying these approaches, the identities of experimental groups remained unknown to the investigator throughout the resistance measurement and data analysis stages. The true identities of the experimental groups were only revealed after the completion of data analysis to ensure objective interpretation of the results.

Immunofluorescence staining

HUVECs were seeded into 8-well chamber slides until they reached 80–90% confluency. After 6 h of tHGA or dexamethasone pretreatment (Chong et al. 2016), the cells were induced with LPS for 6 h and 18 h for the detection of ZO-1 (Qin et al. 2015) and VE-cadherin (Huang et al. 2015), respectively. Immunofluorescence staining was then performed as previously described with modifications (Huang et al. 2015). In details, the cells were then fixed with 4% paraformaldehyde for 15 min, followed by permeabilization with 0.2% Triton X-100 for 15 min. Next, the cells were blocked with 1% BSA in 0.1% Triton X-100 for 30 min prior to overnight primary antibody incubation at 4 °C. On the next day, the cells were incubated with Alexa Fluor 488-conjugated secondary antibody (1:200) for 2 h in the dark at room temperature. Lastly, the cells were mounted with Prolong Gold Antifade Reagent containing 4,6-diamidino-2-phenylindole dihydrochloride (DAPI) and the slides were viewed under a fluorescent microscope (Leica Microsystems, Germany). The gap area was quantified by using ImageJ software (Huang et al. 2015). Briefly, the fluorescent pictures were converted into black and white images, followed by quantification of the junctional protein gap area via the measurement of respective pixilation. The results were then expressed as percentage of gap area.

To avoid biasness, the experimental groups were randomly assigned to wells across the chamber slide. The layout was documented in a separate record, and no treatment labels were marked directly on the chamber slide. Image acquisition and gap area quantification were performed objectively using consistent and standardized microscope and software settings for all samples. Data were analyzed under blinded condition using coded sample identifiers. By applying these approaches, the identity of each experimental group remained unknown to the investigator throughout the staining, imaging, and data analysis stages. The true identities of the experimental groups were only revealed after the completion of data analysis to ensure objective interpretation of the results.

Western Blotting

HUVECs were seeded into 6-well plates until they reach 80–90% confluency. The cells were pretreated with tHGA or dexamethasone for 6 h prior to LPS induction (Chong et al. 2016). Specifically, HUVECs were induced with LPS for 6 h for the detection of ZO-1 and occludin (Qin et al. 2015). For VE-cadherin, the cells were subjected to 18 h of LPS induction (Huang et al. 2015). The induction duration for MAPKs including p38, extracellular signal–regulated kinase (ERK), and c-jun N-terminal kinase (JNK) was 1 h (Guo et al. 2012; Jiang et al. 2013; Qin et al. 2015). For the detection of myosin light chain (MLC) and NF-κB p65, the cells were induced with LPS for 30 min (Zhou et al. 2013) and 2 h (Guo et al. 2012), respectively. After respective induction durations, the cells were lysed with radioimmunoprecipitation assay (RIPA) lysis buffer to obtain whole cell protein lysate (Tham et al. 2010). For the assessment of NF-κB p65 translocation, protein was extracted by using nuclear and cytoplasmic protein extraction reagents according to the manufacturer's protocol. The protein amount was quantified by using BCA protein assay kit according to the manufacturer's protocol. Equal amount of protein was electrophoresed via sodium dodecyl sulfate–polyacrylamide gel electrophoresis (SDS-PAGE) prior to wet transfer onto PVDF membrane. The protocols were performed as previously described with modifications (Tham et al. 2010). In specific, 10 g of protein was used for the SDS-PAGE of junctional proteins (ZO-1, occludin and VE-cadherin). Twenty grams of protein was used for the SDS-PAGE of signalling molecules including MLC, NF-κB p65, p38, ERK, and JNK MAPK. The membrane was then blocked with 5% BSA in Tris-buffered saline with Tween-20 (TBST) for 1 h before overnight incubation with antibody specific for ZO-1 (1:1000), occludin (1:1000), VE-cadherin (1:1000), MLC (1:1000), phospho-MLC (1:1000), NF-κB p65 (1:1000), p38 MAPK (1:1000), phospho-p38 MAPK (1:1000), ERK MAPK (1:1000), phospho-ERK

MAPK (1:1000), JNK MAPK (1:1000), phospho-JNK MAPK (1:1000), lamin (1:1000), and HRP-linked beta-actin (1:10,000) at 4 °C. On the next day, the membrane was incubated with HRP-linked anti-rabbit IgG secondary antibody (1:2500) for 2 h. Lastly, the membrane was incubated with chemiluminescent substrate solution for 1 min before being visualized by using Fusion FX gel documentation system (Vilber Lourmat, Germany). Protein band intensity was quantified by using the ImageJ software and normalized to the loading control (Tham et al. 2010).

To avoid experimental biasness, following protein extraction, all protein samples were re-labelled with randomized codes by an independent individual who was not involved in the experimental procedures. The investigator conducted all subsequent experimental procedures (protein quantification, SDS-PAGE, wet transfer, blocking, antibody incubation, protein visualization, and band quantification) and data analysis using only these coded sample identifiers. By applying these approaches, the identity of each experimental group remained unknown to the investigator throughout the experimental procedures and data analysis stages. The true identities of the experimental groups were only revealed after the completion of data analysis to ensure objective interpretation of the results. To generate a representative blot image with samples arranged in the desired experimental group order, the samples were re-run with known identities after the initial analysis was completed.

Reverse transcription-quantitative polymerase chain reaction (RT-qPCR)

HUVECs were seeded into 6-well plates until they reached 80–90% confluency. The cells were pretreated with tHGA or dexamethasone for 6 h (Chong et al. 2016) before being induced with LPS for 6 h (ZO-1 and occludin) (Qin et al. 2015) or 18 h (VE-cadherin) (Huang et al. 2015). RNA extraction, reverse transcription, and qPCR were performed by using respective kits according to manufacturers' protocols. Housekeeping gene, namely glyceraldehydes-3-phosphate dehydrogenase (GAPDH), was used as the internal control. Forward (F) and reverse (R) primer sequences for each gene were as follows: ZO-1, 5′-TCC GTG TTG TGG ATA CCT TGT A-3′ (F) and 5′-GCC TCG TTC TAC CTC CTT ATG A-3′ (R); occludin, 5′-TAC AGC AAT GGA AAA CCA CAC T-3′ (F) and 5′-CAA AGG AAT GGG AAA CGA CTA A-3′ (R); VE-cadherin, 5′-GCA CCA GTT TGG CCA ATA TA-3′ (F) and 5′-GGG TTT TTG CAT AAT AAG CAG G-3′ (R); GAPDH, 5′-GGC ACA GTC AAG GCT GAG AAT G-3′ (F) and 5′-ATG GTG GTG AAG ACG CCA GTA-3′ (R). The cycling protocol was identical for all primer pairs with an initial activation at 95 °C for 2 min, followed by 40 cycles of denaturation at 95 °C for 5 s and combined annealing/extension at 60 °C for 10 s. The transcriptional fold change of each gene was calculated by using formula $\Delta\Delta Ct = (Ct_{\text{gene of interest}} - Ct_{\text{GAPDH}})_{\text{treated groups}} - (Ct_{\text{gene of interest}} - Ct_{\text{GAPDH}})_{\text{normal group}}$.

To avoid experimental biasness, following RNA extraction, all RNA samples were re-labelled with randomized codes by an independent individual who was not involved in the experimental procedures. The investigator conducted all subsequent experimental procedures (RNA quantification, reverse transcription and qPCR) and data analysis using only these coded sample identifiers. By applying these approaches, the identity of each experimental group remained unknown to the investigator throughout the experimental procedures and data analysis stages. The true identities of the experimental groups were only revealed after the completion of data analysis to ensure objective interpretation of the results.

Molecular docking

The crystal structures of the kinase domain of human ROCK1 in complex with Y-27632, (*R*)-(+)-*trans*−4-(1-Aminoethyl)-*N*-(4-Pyridyl)cyclohexanecarboxamide, were obtained from the Research Collaborator for Structural Bioinformatics Protein Data Bank (RCSB PDB: https://www.rcsb.org/) with PDB ID 2ETR. The structure was determined at 2.60-Å resolution and contained two dimerization domains in the asymmetric unit, including an N-terminal kinase domain and a C-terminal coiled-coil domain, and is in complex with Y-27632 and a peptide substrate (Jacobs et al. 2006). The PDB ID 2ETR structure was selected because it had a well-defined electron density in the ATP binding site and could accommodate ligands from other PDB entries of ROCK1, suggesting that it is a stable and flexible structure that can suit different ligands (Beroza et al. 2022). In the present study, the UCSF Chimera 1.14 package (University of California, SF, USA) (Pettersen et al. 2004) was used to select protein chains, remove water molecules and ligands, and clean up any artefacts. Subsequently, the structure was refined by adding missing atoms, filling missing loop regions, adjusting side-chain conformations, removing alternate conformations, standardizing atom names, and protonating titratable residues using Discovery Studio (DS) 3.1 (Accelrys, Inc., San Diego, CA, USA) (Pettersen et al. 2004).

The molecular docking simulations were performed using CDOCKER protocols within the receptor-ligand interaction section of DS 3.1 (Rullah et al. 2022; Yu et al. 2023). The active sites for the human protein ROCK1 were identified as the binding positions of Y-27632 with a radius of 7.7 Å. During the docking process, multiple conformations of each ligand were generated by performing high-temperature molecular dynamics simulations. Specifically, the ligands were heated to a temperature of 700 K in 2000 steps, followed by a cooling period at 300 K. After this initial heating–cooling phase, the ligands were subjected to refinement using simulated annealing and full force minimization while the receptor

was held rigid. The calculation allowed the ligands to flex and adapt to the binding site while the receptor remained fixed. The generated ligand conformations were clustered based on their binding interactions with the protein. This process enables the identification of the most favorable binding modes and elimination of unlikely binding poses. Finally, the ligand conformation with the highest –CDOCKER interaction energy, a scoring function that evaluates the binding affinity and stability of the ligand–protein complex, was chosen as the best predicted binding mode (Wu et al. 2003).

The 3D structure of the ligand tHGA was built using ChemDraw Professional 15.0 (Perkin Elmer Inc., Waltham, MA, USA) and imported into DS 3.1. The parameters for generating isomers, tautomers, and changing ionization were all set to false, and the ligand was prepared by standardizing charges for common groups, adding hydrogens, enumerating ionization states, ionizing functional groups, removing duplicates, and optimizing with the CHARMm force field in DS 3.1. One ligand of tHGA was generated and used for docking with the human ROCK1.

The validation process involved redocking the original ligands and calculating the heavy atom root mean square deviation (RMSD) of the redocked ligands from the original conformation until most poses had an RMSD ≤ 2.0 Å (Wang et al. 2002). It is important to note that the quality and accuracy of the protein structures and parameters used significantly impact the results of the molecular docking simulations, and it is crucial to follow a rigorous docking protocol (Huang and Zou 2010).

Rescue experiment via TEER assay

A rescue experiment via TEER assay was performed to access if ROCK is important in HUVEC response system to LPS. After confirming this, the TEER response to the incremental addition of tHGA in this pretreatment context was evaluated. TEER assay was conducted as described in the "tHGA preserved endothelial junctional integrity during LPS-induced endothelial hyperpermeability in HUVECs" section. The experimental groups involved in this rescue experiment include:

Experimental Group	tHGA (20 μM)	LPS (1 μg/mL)	ROCK inhibitor Y-27632 (10 μM)
Vehicle control	-	-	-
tHGA control	+	-	-
LPS control	-	+	-
LPS + ROCK inhibitor Y-27632	-	+	+
LPS + tHGA	+	+	-
LPS + tHGA + ROCK inhibitor Y-27632	+	+	+

Statistical analysis

All experiments were performed three times. The results were expressed as mean ± standard error of mean (S.E.M.). Statistical analyses were performed using GraphPad Prism 8. One-way analysis of variance (ANOVA) was conducted, followed by post hoc Dunnet test to compare the difference with the LPS control group. In the present study, $p \leq 0.05$ was considered statistically significant.

Results

tHGA preserved endothelial junctional integrity during LPS-induced endothelial hyperpermeability in HUVECs

TEER reflects the strength of junctional protein complexes between adjacent cells along the endothelial monolayer (Vigh et al. 2021). In the present study, TEER assay was performed to assess the effect of tHGA on endothelial junctional integrity in LPS-induced HUVECs. As shown in Fig. 2, while LPS decreased the TEER value (by 54% compared to the vehicle control group), 20 μM tHGA pretreatment was able to suppress the effect of LPS as indicated by the higher TEER value (by 1.7-fold compared to the LPS control group). This result suggests that tHGA was able to significantly preserve the junctional integrity of HUVEC during LPS induction. For dexamethasone which served as the drug control, 1.6-fold increment in TEER value was observed (Fig. 2). Notably, this effect was comparable to the effect produced by 20 μM tHGA.

For the osmolarity control groups (dextran and PEG300 controls), no significant difference in TEER value was observed between the dextran and PEG300 osmolarity control groups, with the vehicle control group. These results suggest that the possible osmolarity change caused by LPS and tHGA did not affect the TEER values. Therefore, it is deduced that the induction of endothelial junctional disruption by LPS and the inhibition of this disruption by tHGA observed in TEER assay were solely contributed by the effects of LPS and tHGA, respectively.

It is important to note that, although tHGA alone (tHGA control group) did not alter TEER value after 24 h treatment, early-phase changes in endothelial permeability may occur within 1 to 3 h following tHGA treatment. Therefore, additional TEER assay was performed by including the measurements at early time points (0, 1, 3, 6, 12 h) apart from 24 h, following tHGA treatment. The results showed no significant difference in TEER value between these tested time points with 24-h time point and also the normal condition (Figure S1). These findings confirmed that tHGA alone did not

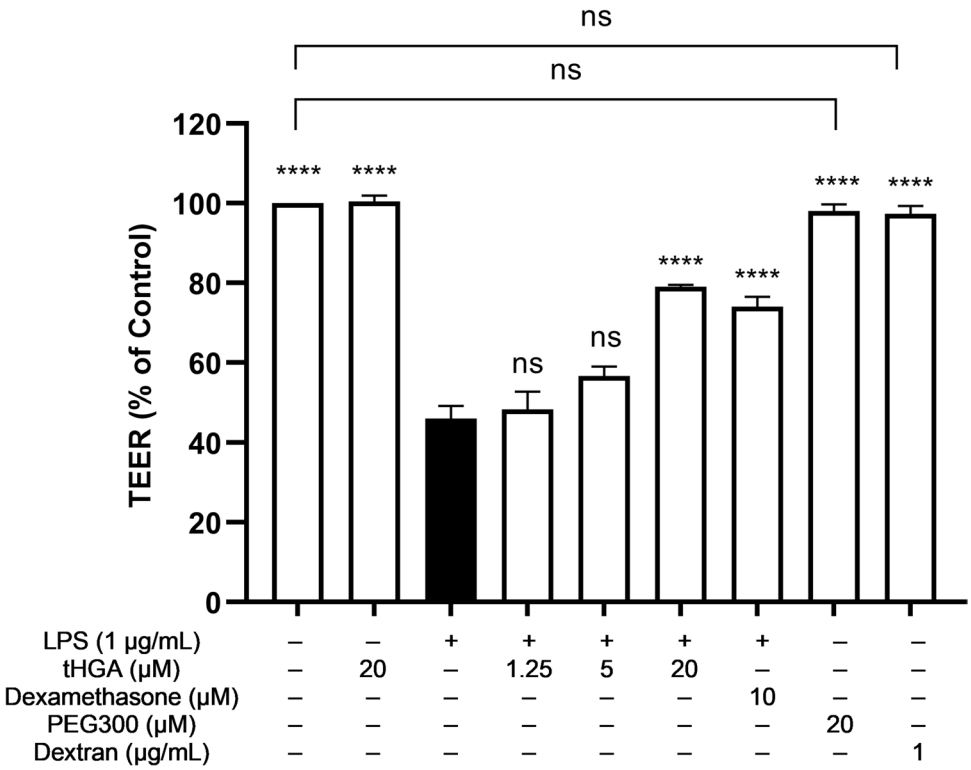

Fig. 2 The effect of 2,4,6-trihydroxy-3-geranyl acetophenone (tHGA) on endothelial junctional integrity in lipopolysaccharide (LPS)-induced Human Umbilical Vein Endothelial Cells (HUVECs). HUVECs were pretreated with different concentrations of tHGA or 10 µM dexamethasone for 6 h prior to 24 h of LPS induction. Data are expressed in mean ± standard error of mean (S.E.M.) of three independent experiments ($n = 3$), with **** representing $p \leq 0.0001$ significantly different from LPS control group

induce immediate or delayed changes in endothelial permeability, thus supporting our original conclusion.

tHGA inhibited delocalization of junctional proteins during LPS-induced endothelial hyperpermeability in HUVECs

In the presence of LPS, junctional proteins that are formerly distributed along cell periphery undergo delocalization, which results in intercellular gap formation (Dorland & Huveneers 2017). Therefore, immunofluorescence staining was conducted to examine the effect of tHGA on the localization of junctional proteins, particularly ZO-1 and VE-cadherin, at cell periphery of LPS-induced HUVECs. Under normal condition, the structure of ZO-1 was intact and there was no intercellular gap along the periphery of endothelial cells (Fig. 3b, i). However, upon LPS induction, ZO-1 displayed marked structural breakages and intercellular gaps along the cell periphery (Fig. 3b, iii). Quantitatively, LPS tremendously induced the formation of intercellular gap by 5.9-fold as compared to the vehicle control group (Fig. 3a). Interestingly, all tested concentrations of tHGA significantly reduced the intercellular gap induced by LPS (Fig. 3b, iv–vi). In comparison to the LPS control group, tHGA inhibited the formation of intercellular gap by 23%, 66%, and 89% at 1.25, 5, and 20 µM, respectively (Fig. 3a). These results suggest that tHGA preserved the intactness of ZO-1 proteins along the endothelial cell periphery by abrogating its delocalization in response to LPS induction in a concentration-dependent manner. The drug control inhibited the ZO-1 intercellular gap formation by 48% which was weaker than the effect exerted by 5 and 20 µM tHGA (Fig. 3a and b, vii).

As shown in Fig. 4a and b, iii, LPS drastically induced the formation of VE-cadherin intercellular gap by 16-fold as compared to the vehicle control group. Similar to ZO-1, a significant reduction in VE-cadherin intercellular gap formation was observed upon pretreatment of tHGA at all concentrations (Fig. 4b, iv–vi). In comparison to the LPS control group, tHGA at 1.25, 5, and 20 µM profoundly suppressed the formation of VE-cadherin intercellular gap by 21%, 72%, and 80%, respectively (Fig. 4a). These results suggest that tHGA also preserved the intactness of VE-cadherin along the endothelial cell periphery in a concentration-dependent manner by suppressing its delocalization in response to LPS induction. In line with the result for ZO-1, dexamethasone attenuated the formation of intercellular gap in VE-cadherin by 64% which was weaker than the effect exerted by 5 and 20 µM tHGA (Fig. 4a and b, vii).

tHGA preserved protein expression of junctional protein in during LPS-induced endothelial hyperpermeability in HUVECs

Apart from inducing delocalization, LPS could also down-regulate junctional protein expression, thus leading to

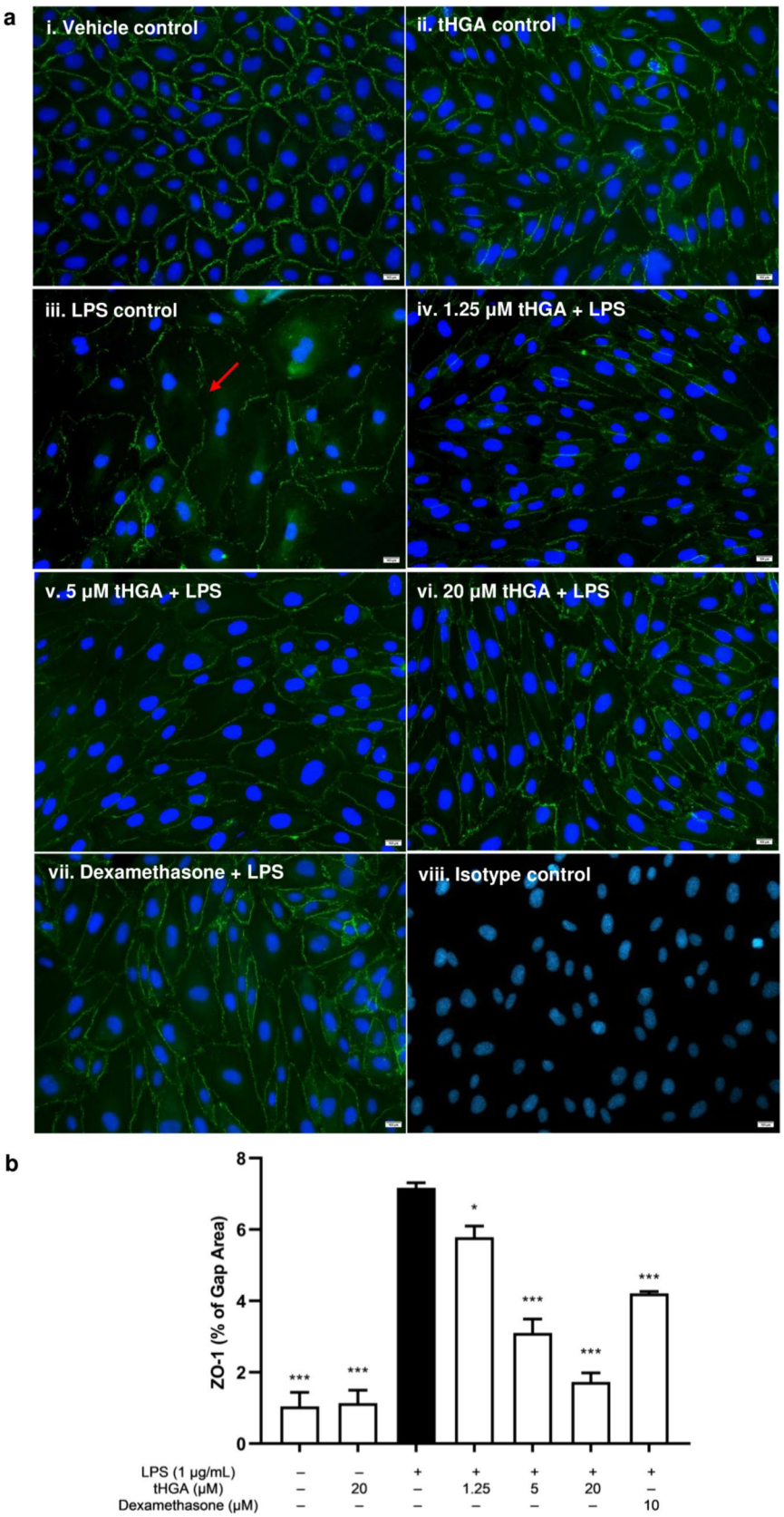

Fig. 3 The effect of 2,4,6-trihydroxy-3-geranyl acetophenone (tHGA) on the localization of zonula occluden (ZO)−1 protein along the cell periphery in lipopolysaccharide (LPS)-induced human umbilical vein endothelial cells (HUVECs). HUVECs were pretreated with different concentrations of tHGA or 10 μM dexamethasone for 6 h prior to 6 h of LPS induction. The degree of localization was expressed in terms of intercellular gap formation which was quantified as **a** percentage of gap area. Data are expressed in mean ± standard error of mean (S.E.M.) of three independent experiments (n = 3), with *** and * representing $p \leq 0.001$ and $p \leq 0.05$ significantly different from the LPS control group, respectively. **b** Representative immunofluorescence images of LPS-induced HUVECs pretreated with different concentrations of tHGA or 10 μM dexamethasone under a fluorescence microscope with 100× magnification. The scale bar of 100 um is provided in each image. Arrow indicates the intercellular gap along the cell periphery

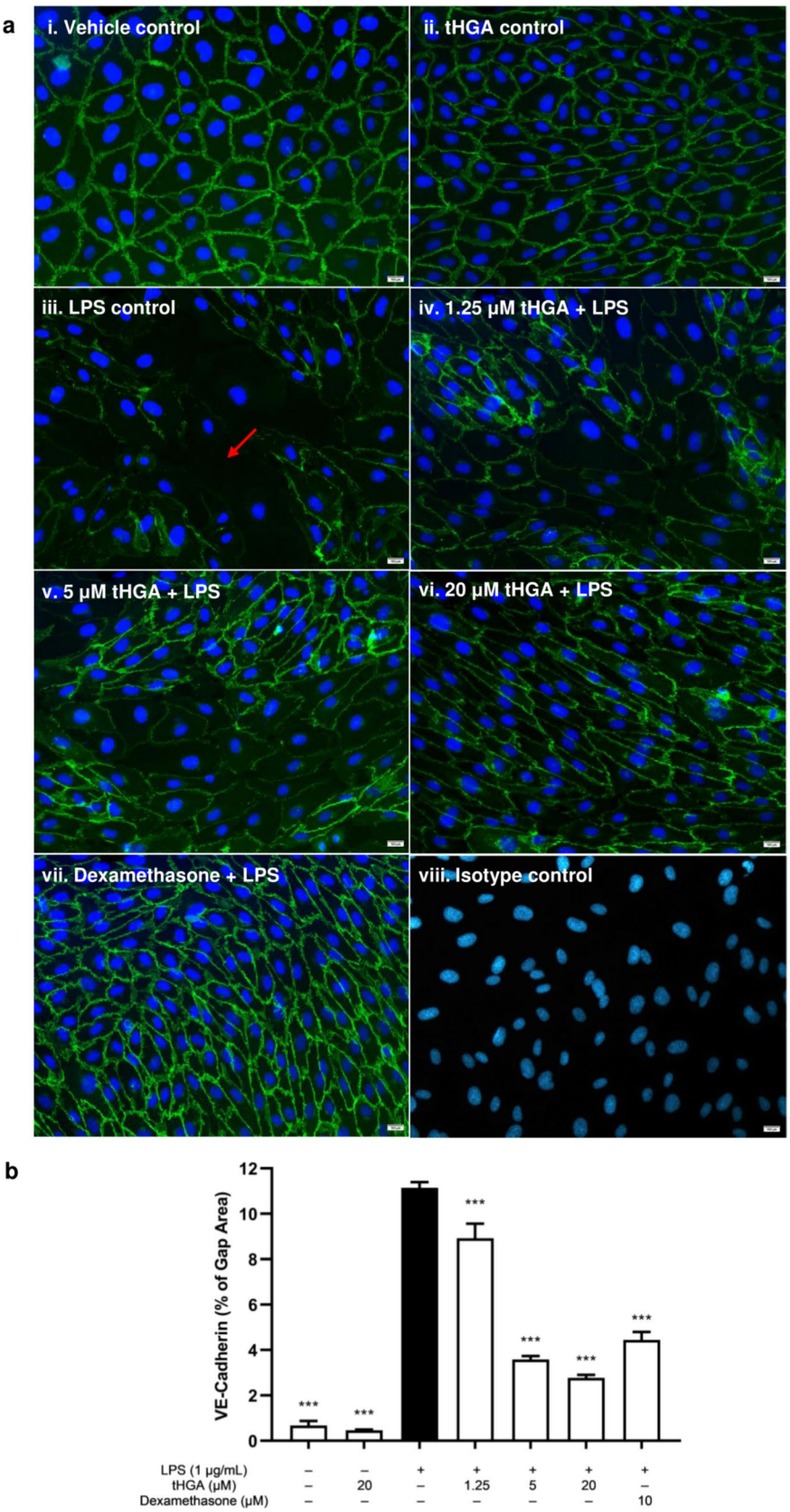

Fig. 4 The effect of 2,4,6-trihydroxy-3-geranyl acetophenone (tHGA) on the localization of vascular endothelial (VE)-cadherin protein along the cell periphery in lipopolysaccharide (LPS)-induced human umbilical vein endothelial cells (HUVECs). HUVECs were pretreated with different concentrations of tHGA or 10 µM dexamethasone for 6 h prior to 18 h of LPS induction. The degree of localization was expressed in terms of intercellular gap formation which was quantified as **a** percentage of gap area. Data are expressed in mean ± standard error of mean (S.E.M.) of three independent experiments ($n = 3$), with *** representing $p \leq 0.001$ significantly different from the LPS control group. **b** Representative immunofluorescence images of LPS-induced HUVECs pretreated with different concentrations of tHGA or 10 µM dexamethasone under a fluorescence microscope with 100× magnification. The scale bar of 100 um is provided in each image. Arrow indicates the intercellular gap along the cell periphery

impaired endothelial junctional integrity (Liu et al. 2015). Therefore, Western Blotting was carried out to evaluate the effect of tHGA on the expression of junctional proteins at protein level in LPS-induced HUVECs.

As shown in Fig. 5a, LPS control group displayed significant downregulation of ZO-1 protein expression (by 53% compared to the vehicle control group). However, 5 and 20 μM tHGA pretreatments were able to profoundly abrogate the effect of LPS as indicated by the higher expression ratio (by 2.2-fold and threefold, respectively, compared to the LPS control group) (Fig. 5a). These results suggest that tHGA was able to preserve the expression of ZO-1 at protein level during LPS induction. Dexamethasone which was the drug control demonstrated 2.5-fold increment in ZO-1 expression, which was comparable to the effect produced by 5 μM tHGA (Fig. 5a).

In the presence of LPS, the protein expression of occludin was drastically down regulated by 63% as compared to the vehicle control group (Fig. 5b). Interestingly, 20 μM tHGA pretreatment was able to alleviate the effect of LPS as indicated by the higher expression ratio (by 3.3-fold compared to the LPS control group) (Fig. 5b). This result indicates that tHGA was capable of preserving the expression of occludin at protein level during LPS induction. Dexamethasone increased the expression of occludin by 2.8-fold as compared

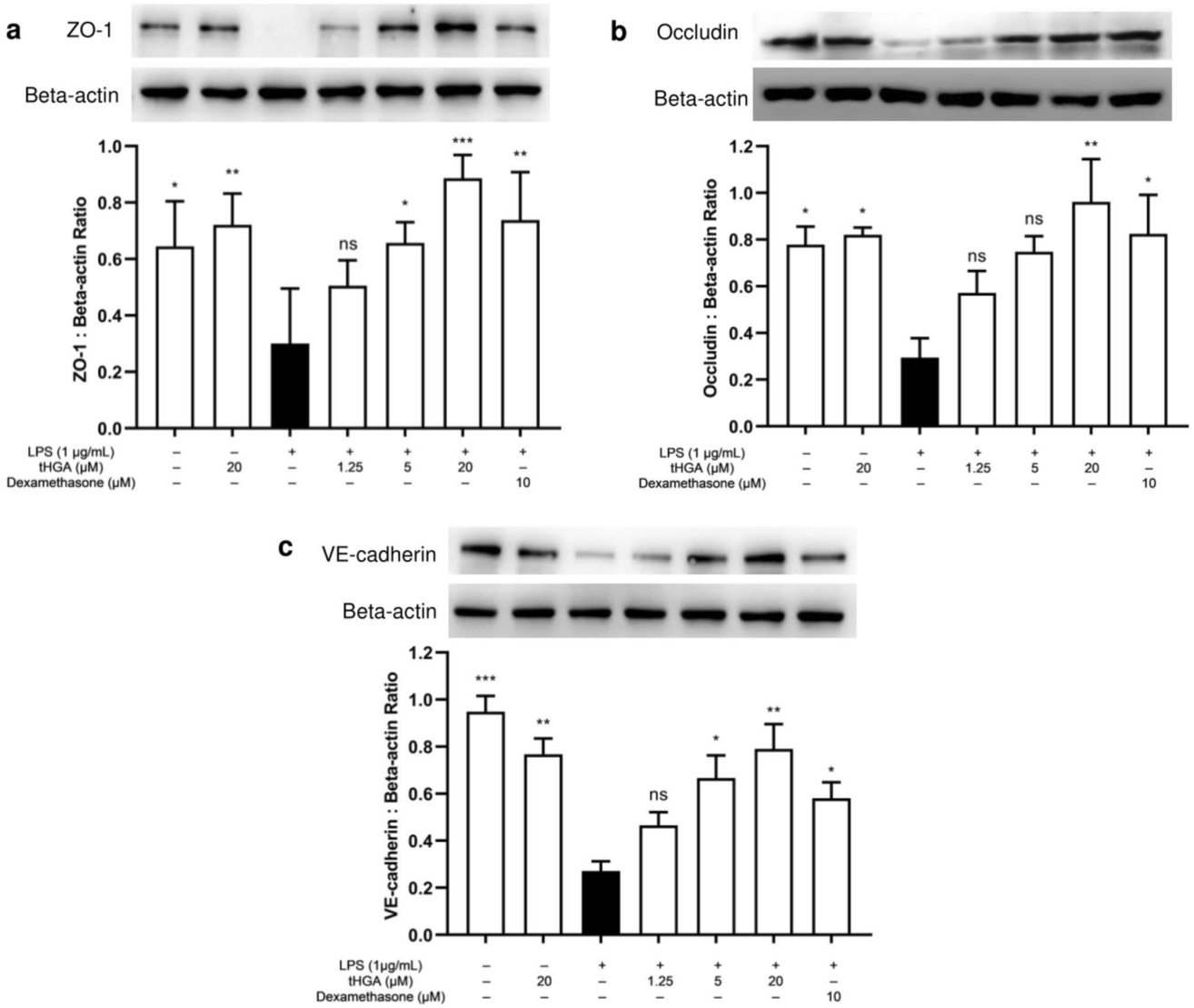

Fig. 5 The effect of 2,4,6-trihydroxy-3-geranyl acetophenone (tHGA) on protein expression of **a** zonula occluden (ZO)−1, **b** occludin, and **c** vascular endothelial (VE)-cadherin in lipopolysaccharide (LPS)-induced human umbilical vein endothelial cells (HUVECs). HUVECs were pretreated with different concentrations of tHGA or 10 μM dexamethasone for 6 h prior to 6 or 18 h of LPS induction. Data are expressed in mean ± standard error of mean (S.E.M.) of three independent experiments (n = 3), with ***, **, and * representing $p \leq 0.001$, $p \leq 0.01$, and $p \leq 0.05$ significantly different from the LPS control group, respectively

to the LPS control group (Fig. 5b). Notably, the inhibitory effect exerted by 5 μM tHGA was not significant.

As shown in Fig. 5c, LPS profoundly downregulated the expression of VE-cadherin by 72% as compared to the vehicle control group. However, 5 and 20 μM tHGA were able to significantly suppress the effect of LPS as indicated by the higher expression ratio (by 2.5-fold and 2.9-fold, respectively, compared to the LPS control group) (Fig. 5c). These results imply that tHGA was able to preserve the expression of VE-cadherin at protein level during LPS induction. About 2.1-fold increment in VE-cadherin expression was produced by dexamethasone (Fig. 5c). Notably, this effect was weaker than the effect produced by 5 μM tHGA.

In addition, Western Blotting was also performed to examine the effects of tHGA at all test concentrations (1.25, 5 and 20 μM) on the expression of all test junctional proteins (ZO-1, occludin, and VE-cadherin) under non-LPS-induced condition. The results showed that there was no significant difference between each tHGA's test concentration with the vehicle control (normal condition), for all junctional protein expression (Fig. S2). Also, there was no significant difference among each tHGA's test concentration on the expression of all test junctional proteins (Fig. S2). These findings suggest that tHGA at all test concentrations did not regulate the expression of all test junctional proteins.

tHGA preserved gene expression of junctional proteins during LPS-induced endothelial hyperpermeability in HUVECs

tHGA has been shown to significantly inhibit the downregulation of junctional protein expression at protein level. Therefore, further investigation on gene expression was performed by reverse transcription-quantitative polymerase chain reaction (RT-qPCR) to assess the effect of tHGA on the gene expression of junctional proteins in LPS-induced HUVECs.

As shown in Fig. 6a, LPS profoundly downregulated the gene expression of ZO-1 by 77% as compared to the vehicle control group. Significantly, 5 and 20 μM tHGA were able suppress the effect of LPS as indicated by the higher fold change (by threefold and 3.4-fold, respectively, compared to the LPS control group) (Fig. 6a). These results suggest that tHGA was able to preserve the gene expression of ZO-1 during LPS induction. About 2.8-fold increment in ZO-1 gene expression was observed in dexamethasone drug control group as compared to the LPS control group (Fig. 6a). Notably, the effect produced by dexamethasone was comparable to the effect produced by 5 μM tHGA.

In the presence of LPS, the gene expression of occludin was aberrantly downregulated by 76% as compared to the vehicle control group (Fig. 6b). Interestingly, 20 μM tHGA pretreatment was capable of inhibiting the effect of LPS as indicated by the higher fold change (by 3.2-fold compared to the LPS control group) (Fig. 6b). This result implies that tHGA was capable of preserving the gene expression of occludin during LPS induction. In comparison to the LPS control group, 10 μM dexamethasone demonstrated 2.5-fold increment in occludin gene expression (Fig. 6b). Notably, in line with the results of Western Blotting, both 1.25 μM and 5 μM tHGA did not exert significant inhibitory effect on the downregulation of occludin's gene expression.

As demonstrated in Fig. 6c, the gene expression of VE-cadherin was drastically downregulated by LPS by 80% as compared to the vehicle control group. Despite this detrimental condition, tHGA pretreatments at 5 and 20 μM were able to tremendously alleviate the effect of LPS as indicated by the higher fold change (by 2.7-fold and 3.4-fold, respectively, compared to the LPS control group) (Fig. 6c). These results indicate that tHGA was able to preserve the gene expression of VE-cadherin during LPS induction. The drug control effectively restored the gene expression of VE-cadherin threefold, which was comparable to the effect produced by 5 μM tHGA (Fig. 6c).

tHGA inhibited the activation of MLC, NF-κB p65, p38 MAPK, and ERK MAPK but not JNK MAPK during LPS-induced endothelial hyperpermeability in HUVECs

Western Blotting was performed to elucidate the effects of tHGA on several signalling molecules along GEF-H1/RhoA/ROCK pathway, the major signal transduction pathway mediating junctional protein disruption in response to LPS induction.

To determine whether GEF-H1/RhoA/ROCK pathway underlies the protective effects of tHGA on LPS-induced endothelial hyperpermeability, the effect of tHGA on phosphorylation of MLC, the most downstream signalling molecule in this pathway, was examined. As shown in Fig. 7a, LPS aberrantly phosphorylated MLC by 6.8-fold as compared to the vehicle control group. Upon 20 μM tHGA pretreatment, the phosphorylation of MLC was significantly reduced by 60% as compared to the LPS control group (Fig. 7a). This result implies that GEF-H1/RhoA/ROCK pathway was involved in mediating the protective effects of tHGA during LPS-induced endothelial hyperpermeability. Moreover, the ROCK inhibitor, Y-27632, markedly abolished LPS-induced MLC phosphorylation by 79% (Fig. 7a), validating that MLC indeed acts downstream of ROCK in the GEF-H1/RhoA/ROCK pathway.

As shown in Fig. 7b, NF-κB p65 subunits mainly resided in the cytoplasm instead of nucleus under normal condition. Conversely, in the presence of LPS, the expression of NF-κB p65 was increased by 1.8-fold in the nucleus (Fig. 7b, i) while decreased by 52% in the cytoplasm (Fig. 7b, ii). These

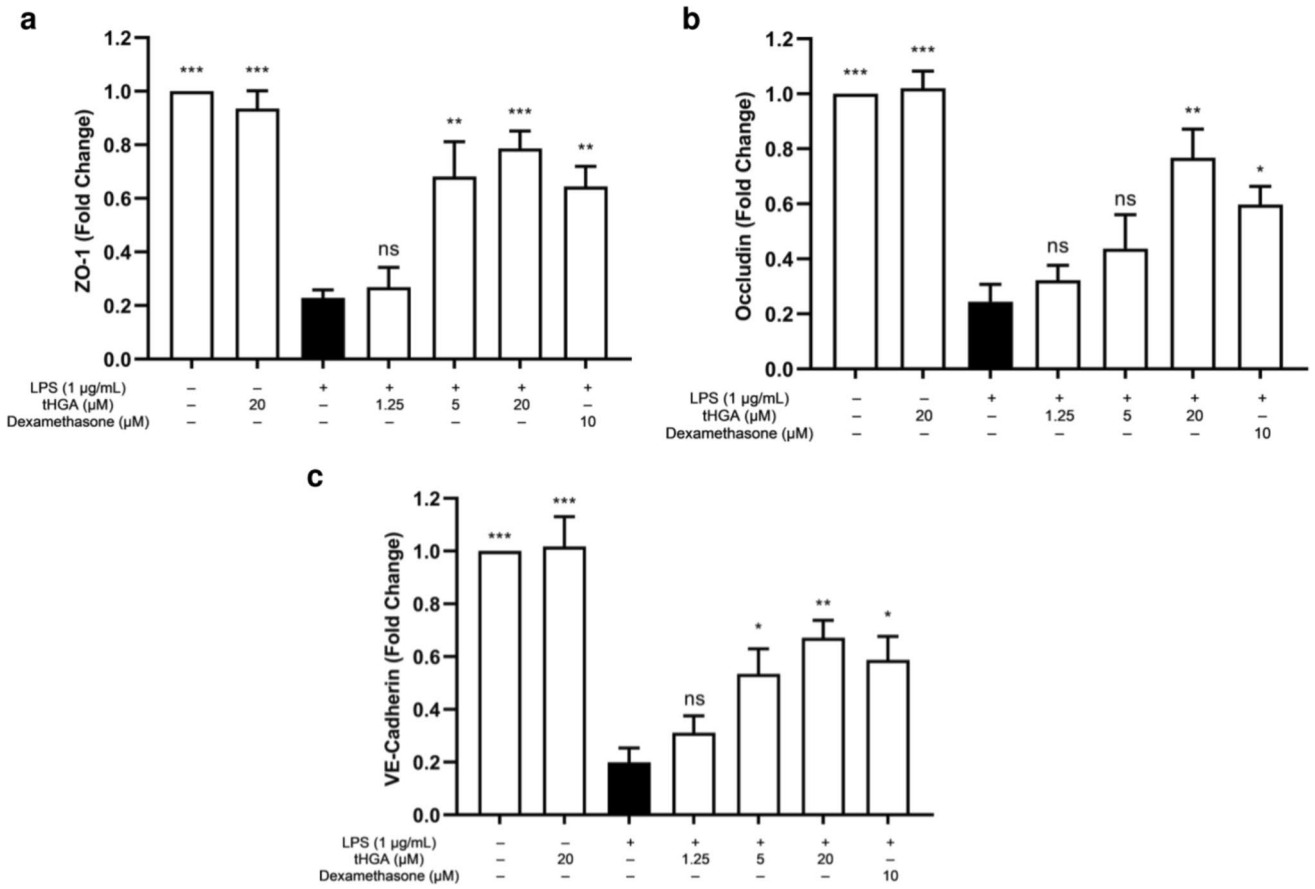

Fig. 6 The effect of 2,4,6-trihydroxy-3-geranyl acetophenone (tHGA) on gene expression of **a** zonula occluden (ZO)−1, **b** occludin, and **c** vascular endothelial (VE)-cadherin in lipopolysaccharide (LPS)-induced human umbilical vein endothelial cells (HUVECs). HUVECs were pretreated with different concentrations of tHGA or 10 μM dexamethasone for 6 h prior to 6 or 18 h of LPS induction. Data are expressed in mean ± standard error of mean (S.E.M.) of three independent experiments (n = 3), with ***, **, and * representing $p \leq 0.001$, $p \leq 0.01$, and $p \leq 0.05$ significantly different from the LPS control group, respectively

results indicate that LPS induced the drastic translocation of NF-κB p65 subunits from the cytoplasm into the nucleus. However, upon pretreatment of 20 μM tHGA, the expression of NF-κB p65 was lowered by 79% in the nucleus (Fig. 7b, i) while increased 2.1-fold in the cytoplasm (Fig. 7b, ii) as compared to the LPS control group. These results suggest that inhibition of NF-κB p65 translocation mediates the protective effect of tHGA against LPS-induced endothelial hyperpermeability. Besides that, NF-κB p65 inhibitor, namely BAY 11–7082, effectively dampened the translocation of NF-κB p65 subunits, as evidenced by 97% reduction (Fig. 7b, i) and twofold increment (Fig. 7b, ii) of NF-κB p65 expression in nucleus and cytoplasm, respectively.

LPS induction activates several MAPKs including p38, ERK, and JNK. Figure 7c–e show that the levels of phosphorylated p38 MAPK, ERK, and JNK were elevated by 2.2-fold, 1.3-fold, and 0.8-fold, respectively, as compared to the vehicle control group. However, upon 20 μM tHGA pretreatment, the phosphorylation levels of p38 MAPK and ERK were significantly inhibited by 75% and 65%, as compared to the LPS control group (Fig. 7c–d). However, the LPS-induced p38 MAPK and ERK phosphorylation was aberrantly suppressed by their respective inhibitors, namely SB203580 and PD98059, where approximately 80% reduction was observed (Fig. 7c, d). These results imply that the inactivation of p38 and ERK MAPK pathways played a role in the manifestation of tHGA protective effects during LPS-induced endothelial hyperpermeability. While the JNK MAPK inhibitor, namely SP600125, completely abolished the phosphorylation of JNK as compared to the LPS control group, pretreatment of 20 μM tHGA failed to inhibit the activation of JNK MAPK (Fig. 7e). This result indicates that JNK MAPK pathway was not involved in mediating the protective effects of tHGA during LPS-induced endothelial hyperpermeability.

tHGA predictably targeted on ROCK1 during LPS-induced endothelial hyperpermeability in HUVECs

Since MLC, NF-κB p65, p38 MAPK, and ERK MAPK diverge significantly from the GEF-H1/RhoA/ROCK pathway, an in silico investigation was conducted to gain insights into the molecular target of tHGA. The aim was to explore whether the proposed expressional regulator of tHGA could potentially interact with ROCK1, a key protein from the GEF-H1/RhoA/ROCK pathway. A molecular docking study was performed to predict the binding affinity and potential interaction between tHGA and ROCK1. The CDOCKER protocol was first validated as the most acceptable method for docking tHGA to the binding site of the co-crystallized inhibitor, Y-27637, in human ROCK1 (PDB ID 2ETR). The validation process revealed that CDOCKER had the lowest RMSD value of 0.53 Å (Fig. 8a), indicating that the docking program accurately predicted the ligand's binding mode. Additionally, ten conformations of the co-crystallized inhibitor were generated, and the results indicated that the RMSD values were below 2.0 Å (Wang et al. 2002).

The docking analysis of tHGA revealed ten conformations that exhibited CDOCKER interaction energy similar to that of its co-crystallized ligand, Y-27637. Specifically, the average CDOCKER interaction energies of tHGA and Y-27637 were − 39.30 kcal/mol and − 39.25 kcal/mol, respectively (Fig. 8b). Notably, the co-crystallized ligand demonstrated high potency as a ROCK1 inhibitor, with a Ki value of 0.15 μM (Jacobs et al. 2006). Furthermore, the docking results indicated that tHGA formed significant binding interactions with the active site of human ROCK1, with its carboxylate group interacting with Met156 and Glu154 side chains at distances of 2.15 Å and 3.05 Å, respectively. These binding interactions were similar to those observed in the co-crystallized ligand, where the pyridine nitrogen of Y-27637 formed a hydrogen bond with the amide nitrogen of Met156 at a distance of 2.07 Å, and an aromatic carbon donated a hydrogen bond to the Glu154 main chain carbonyl at a distance of 3.60 Å (Pierce et al. 2002). In addition, the carboxylate group of tHGA formed a hydrogen bond interaction with Tyr155, with a distance of 2.72 Å. Importantly, Met156 and Glu154 are crucial amino acid residues involved in stabilizing the protein-inhibitor complex within the active site of human ROCK1 (Shen et al. 2015). Thus, these findings suggest that tHGA may directly bind to human ROCK1, and its ability to interact with key amino acid residues involved in stabilizing the protein-inhibitor complex may contribute to its efficacy. Future research is required to elucidate the experimental mechanism of tHGA direct inhibition of ROCK1 and its potential therapeutic applications.

ROCK was important in HUVEC response system to LPS, and tHGA was validated to target on ROCK

The results of Western Blotting demonstrated that ROCK inhibition significantly suppressed the phosphorylation of MLC (Fig. 7(b)). MLC is the downstream molecule of ROCK and its phosphorylation is responsible for the manifestation of junctional protein disruption during LPS induction. As the ultimate aim of suppression of junctional protein disruption is to preserve endothelial junctional integrity during LPS induction, and computer modelling via molecular docking has predicted ROCK as the molecular target of tHGA, it is important to further assess if ROCK inhibition exerts beneficial effect to the LPS-induced decrease in TEER value. To test this, a rescue experiment via TEER assay was performed.

The results showed that the inhibition of ROCK (indicated by the "LPS + ROCK inhibitor Y-27632" group, colored in blue) significantly restored the LPS-induced TEER reduction by 1.8-fold (Fig. 9), suggesting the importance of ROCK in HUVEC response system to LPS. After confirming this, the TEER response to the incremental addition of tHGA in this pretreatment context was further examined. The results demonstrated that the combination of tHGA treatment and ROCK inhibition (indicated by the "LPS + tHGA + ROCK inhibitor Y-27632" group, colored in red) promisingly restored the LPS-induced TEER reduction by 2.1-fold (Fig. 9). Notably, this effect was significantly stronger than the effects exerted by sole ROCK inhibition (indicated by the "LPS + ROCK inhibitor Y-27632" group, colored in blue) and sole tHGA treatment (indicated by the "LPS + tHGA" group, colored in green) (Fig. 9). This additive effect on the overall preservation of endothelial junctional integrity as measured by TEER promisingly validated that ROCK was a prominent element in HUVEC intracellular signal transduction cascade in response to LPS, and tHGA precisely targeted on it to exhibit its endothelial junctional protective effects.

Discussion

Under normal physiological conditions, endothelium acts as a functional barrier in maintaining homeostasis at an optimal level, including the regulation of vascular permeability, inflammation, hemostasis, and vascular tone (Daiber et al. 2017). Alarmingly, LPS-induced hyperinflammatory responses consequently provoke endothelial hyperpermeability accompanied by an unrestricted passage of plasma proteins across the endothelium as a result of compromised junctional integrity. These events ultimately lead to excessive fluid leakage, endothelial dysfunction, multiple organ

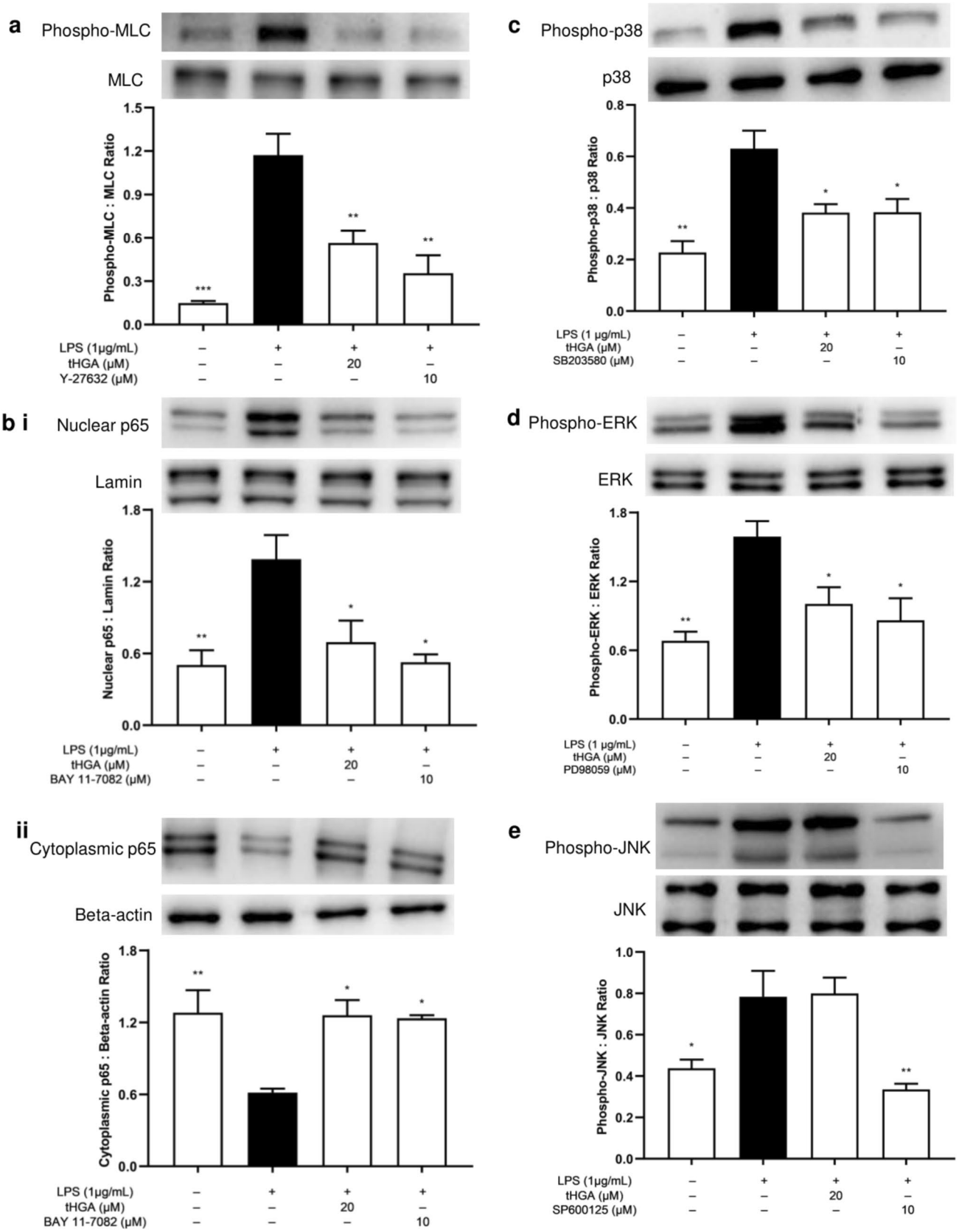
a
Phospho-MLC
MLC
Phospho-MLC : MLC Ratio
1.5
1.2
0.9
0.6
0.3
0.0
***
**
**
LPS (1μg/mL) – + + +
tHGA (μM) – – 20 –
Y-27632 (μM) – – – 10
c
Phospho-p38
p38
Phospho-p38 : p38 Ratio
0.8
0.6
0.4
0.2
0.0
**
*
*
LPS (1 μg/mL) – + + +
tHGA (μM) – – 20 –
SB203580 (μM) – – – 10
b i
Nuclear p65
Lamin
Nuclear p65 : Lamin Ratio
1.8
1.2
0.6
0.0
**
*
*
LPS (1μg/mL) – + + +
tHGA (μM) – – 20 –
BAY 11-7082 (μM) – – – 10
d
Phospho-ERK
ERK
Phospho-ERK : ERK Ratio
1.8
1.2
0.6
0.0
**
*
*
LPS (1 μg/mL) – + + +
tHGA (μM) – – 20 –
PD98059 (μM) – – – 10
ii
Cytoplasmic p65
Beta-actin
Cytoplasmic p65 : Beta-actin Ratio
1.8
1.2
0.6
0.0
**
*
*
LPS (1μg/mL) – + + +
tHGA (μM) – – 20 –
BAY 11-7082 (μM) – – – 10
e
Phospho-JNK
JNK
Phospho-JNK : JNK Ratio
1.0
0.8
0.6
0.4
0.2
0.0
*
**
LPS (1μg/mL) – + + +
tHGA (μM) – – 20 –
SP600125 (μM) – – – 10

◂**Fig. 7** The effect of 2,4,6-trihydroxy-3-geranyl acetophenone (tHGA) on **a** myosin light chain (MLC) phosphorylation, **b** nuclear factor kappa-light-chain-enhancer of activated B cells (NF-κB) p65 translocation, **c** p38 mitogen-activated protein kinase (MAPK) phosphorylation, **d** extracellular signal-regulated kinase (ERK) MAPK phosphorylation, and **e** c-jun N-terminal kinase (JNK) MAPK phosphorylation in lipopolysaccharide (LPS)-induced human umbilical vein endothelial cells (HUVECs). HUVECs were pretreated with tHGA for 6 h or the indicated inhibitors of respective signaling pathways prior to their respective hours of LPS induction. Data are expressed in mean ± standard error of mean (S.E.M.) of three independent experiments (n = 3), with ***, **, and * representing $p \leq 0.001$, $p \leq 0.01$, and $p \leq 0.05$ significantly different from the LPS control group, respectively

failures, and septic shock if the condition is prolonged and left uncontrolled (Li et al. 2017).

Our previous in vivo study revealed that tHGA was capable of inhibiting vascular leakage in a murine model of LPS-induced BALB/c mice (Chan et al. 2021). In vitro, our previous study using LPS-induced HUVECs demonstrated that tHGA significantly abrogated endothelial hyperpermeability via both paracellular and transcellular routes. Mechanistically, this inhibitory effect was contributed by the attenuation of F-actin cytoskeletal rearrangement during LPS induction (Chong et al. 2016). As the paracellular route is more prevalent for the permeation of particles across the endothelium, and F-actin cytoskeleton, the key player of this route, was shown to be regulated by tHGA during LPS induction, it prompted the further investigation on the junctional protein complexes which anchor and collaborate with F-actin cytoskeleton in preserving paracellular endothelial integrity (Vestweber et al. 2014).

To test this, TEER assay was performed to examine the effect of tHGA on the integrity of junctional protein complexes along LPS-induced HUVEC monolayer. Junctional integrity refers to the strength of junctional protein complexes that interconnect adjacent endothelial cells along the monolayer (Vigh et al. 2021). A high TEER value corresponds to high junctional integrity, indicating that the endothelial cells are tightly connected by junctional protein complexes in order to constitute an intact monolayer without intercellular gaps (Vigh et al. 2021). The result showed that 20 μM tHGA significantly preserved endothelial junctional integrity of HUVEC monolayer in the presence of LPS. As junctional protein complexes govern paracellular permeability, this result further validates the finding of a previous study which demonstrated that tHGA exerted significant inhibitory effect against paracellular permeability during LPS induction (Chong et al. 2016). Taken together, the attenuation of paracellular permeability by tHGA reported previously seems to be attributed to the ability of tHGA to preserve endothelial junctional integrity during LPS induction.

The persistent challenge of LPS is capable of exacerbating endothelial junctional integrity through rearrangement of cortical F-actin, leading to the formation of stress fiber excessively (Dudek and Garcia 2001). F-actin cytoskeleton mainly exists in a cortical form which tightly anchors to junctional proteins along the cell periphery in order to maintain endothelial structural integrity (Prasain and Stevens 2009). Alarmingly, overwhelming actomyosin contraction of stress fiber could generate a relatively strong cytoskeletal pulling tension which pulls the cytoskeleton-anchored junctional proteins away from the cell periphery (Dorland and Huveneers 2017; Schnoor et al. 2017). These series of events consequently lead to delocalization of junctional proteins, ultimately forming structural breakages or intercellular gaps along the cell periphery (Huang et al. 2015; Yang et al. 2015). Chong et al. (2016) demonstrated that tHGA was capable of inhibiting F-actin cytoskeletal rearrangement through attenuation of stress fiber formation, thus leading to attenuation of LPS-induced endothelial hyperpermeability. Therefore, immunofluorescence staining was conducted to elucidate the effect of tHGA on the localization of junctional proteins, particularly ZO-1 and VE-cadherin, along the endothelial cell periphery in the presence of LPS. In this assay, the percentage of intercellular gap formation serves as the indicator for the degree of junctional protein delocalization. Based on the results, tHGA at all tested concentrations profoundly attenuated intercellular gap formation by preserving intact ZO-1 and VE-cadherin along the endothelial cell periphery. These results imply that abrogation of junctional protein delocalization was one of the mechanisms by which tHGA protects against LPS-induced endothelial hyperpermeability. It is important to highlight that the effect of tHGA on the localization of occludin was not included in the present study due to unavailability of occludin antibody which gives satisfactory immunofluorescence signals during the staining process. It is also significant to note that the LPS control group contained fewer cells in comparison to other experimental groups as the cell monolayer appeared to peel off and moved freely in the culture medium, most likely attributed to the loss or disruption of junctional proteins at the cell periphery. Despite these limitations, the promising findings of immunofluorescence staining somehow indicated that the preservation of both intact ZO-1 and VE-cadherin is one of the key factors contributing to the preservation of endothelial junctional integrity during LPS induction.

Another molecular mechanism that could contribute to LPS-induced endothelial hyperpermeability is the down-regulation of junctional protein expression (Liu et al. 2015). This mechanism is distinct from junctional protein delocalization and is regulated by post-translational phosphorylation of junctional proteins (Rao 2009). Both these mechanisms can occur independently or simultaneously. The findings of immunofluorescence staining proved that tHGA profoundly preserved intact junctional proteins along the cell periphery by inhibiting their delocalization during LPS induction. The

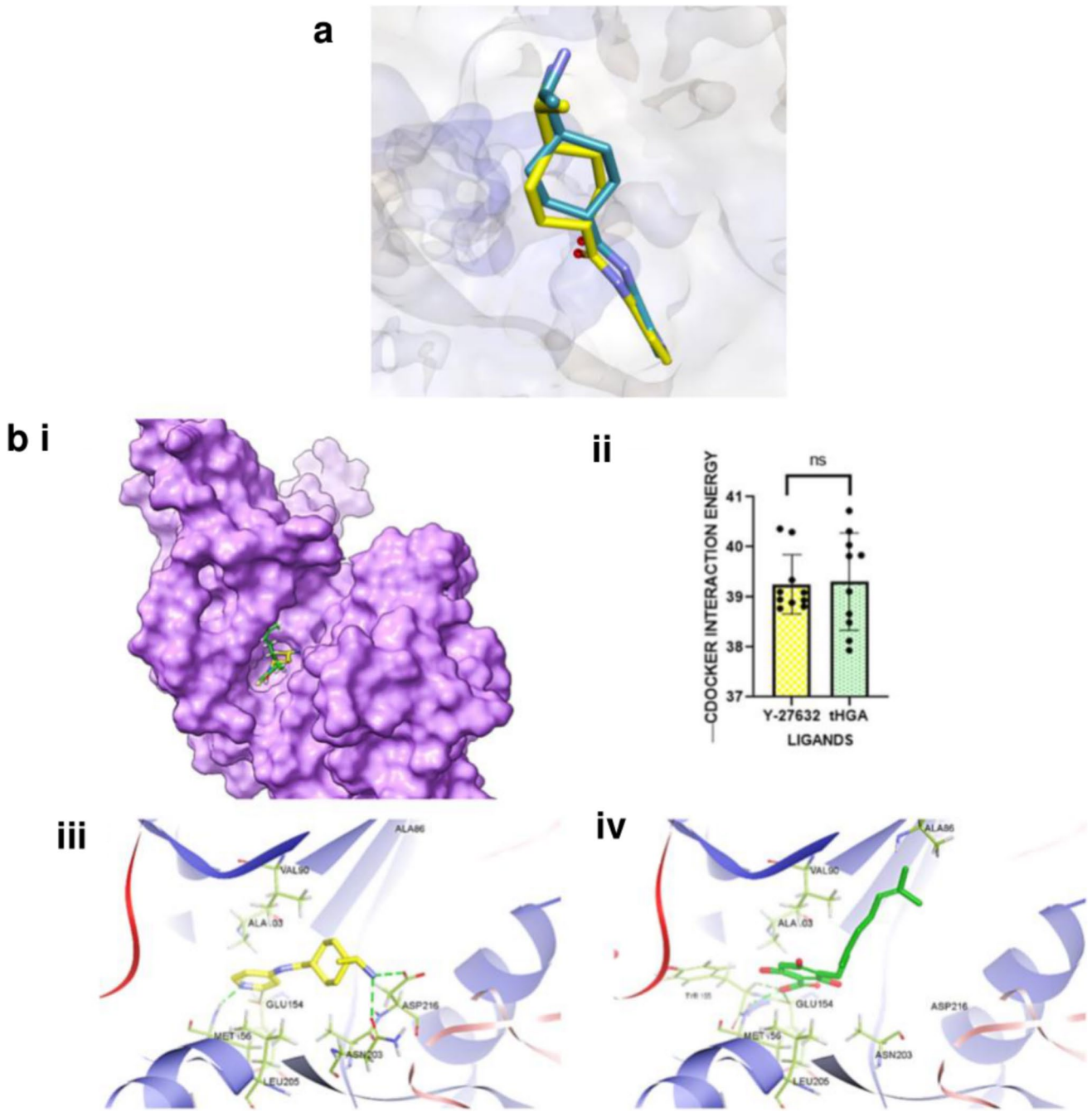

Fig. 8 **a** Superposition of the redocked conformation of Y-27632 over the co-crystallized ligand Y-27632 retrieved from the protein crystal structure. The original Y-27632 is in yellow, and the redocked Y-27632 is in cyan; **b** superimposition of two ligand poses: co-crystallized **i** Y-27632 and 2,4,6-trihydroxy-3-geranyl acetophenone (tHGA) docking pose, with **ii** average CDOCKER interaction energies calculated over ten conformations in the active site of human ROCK1 (PDB ID 2ETR). The significance of the differences between groups was determined using one-way ANOVA, followed by an unpaired Student's *t*-test with $p \leq 0.05$. (n.s. is non-significant). The essential binding interactions between **iii** Y-27637 and **iv** tHGA in the active site of human ROCK1

present study demonstrates that tHGA's ability to preserve endothelial junctional integrity depends on the simultaneous inhibition of both delocalization and downregulation of junctional protein expression. In particular, both 5 and 20 μM tHGA showed marked effects in preserving the expression of ZO-1 and VE-cadherin at protein level during LPS induction. Notably, it is worth mentioning that LPS-induced VE-cadherin disruption could result in either unchanged or reduced protein expression, depending on the concentration, induction duration, and serotype of LPS used

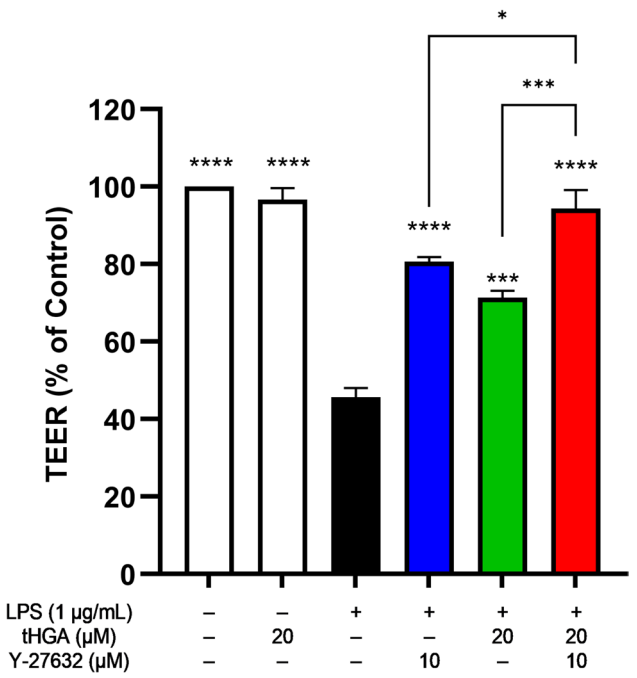

Fig. 9 The effect of ROCK inhibition only, 2,4,6-trihydroxy-3-geranyl acetophenone (tHGA) only, and the combined effect of ROCK inhibition and tHGA, on endothelial junctional integrity in lipopolysaccharide (LPS)-induced human umbilical vein endothelial cells (HUVECs). HUVECs were pretreated with tHGA or ROCK inhibitor Y-27632 or both for respective durations prior to 24 h of LPS induction. Data are expressed in mean ± standard error of mean (S.E.M.) of three independent experiments (n = 3), with ****, ***, and * representing $p \leq 0.0001$, $p \leq 0.01$, and $p \leq 0.05$ significantly different from LPS control group, respectively

(Chan et al. 2020). In the present study, the observed reduction of VE-cadherin expression was due to the induction of LPS at 1 µg/mL for 18 h. This result is in line with the review findings of Chan et al. (2020) which reported that inducing cells with LPS derived from *E. coli* at 1 µg/mL or higher concentrations for at least 6 h could disrupt VE-cadherin by reducing its expression. It is important to highlight that only 20 µM tHGA was able to significantly preserve the protein expression of occludin during LPS induction. This discrepancy could be due to the possibility that tHGA exerted more prominent effects in preserving the protein expression of ZO-1 and VE-cadherin rather than occludin. In contrary to ZO-1 and VE-cadherin which reside intracellularly, occludin is located in the transmembrane space between adjacent endothelial cells (Guo et al. 2018; Komarova et al. 2017). Elevated tyrosine phosphorylated and Ser/Thr dephosphorylated occludin could lose interaction with other junctional proteins such as ZO-1 and VE-cadherin, resulting in junctional protein dissociation (Basuroy et al. 2003; Kale et al. 2003; Rao 2009; Seth et al. 2007). The role of occludin in maintaining junctional integrity may explain our findings on the TEER assay which demonstrated that 5 µM tHGA failed to preserve LPS-induced endothelial junctional integrity, as tHGA at the same concentration significantly preserved the protein expression of both ZO-1 and VE-cadherin but not occludin.

Besides that, while the expression of glucocorticoid receptor in HUVECs is relatively low leading to partial TEER recovery (Wang et al. 2015), the results of Western Blotting showed that dexamethasone fully restored the expression of ZO-1 and occludin during LPS induction. This scenario could be arisen from several factors. Although glucocorticoid receptor level in HUVECs is relatively low, the receptor is still present and can mediate genomic responses (Löwenberg et al. 2008), especially in the presence of a potent synthetic glucocorticoid like dexamethasone, which has high glucocorticoid receptor binding affinity (Lammer et al. 2023). It is possible that even low glucocorticoid receptor expression is sufficient to induce the transcriptional upregulation or preservation of junctional proteins such as ZO-1 and occludin, particularly if these genes are highly sensitive to glucocorticoid receptor activation (Stahn et al. 2007). Additionally, the preservation of ZO-1 and occludin expression may require a lower threshold of glucocorticoid receptor signalling than the complex physiological process of restoring TEER (Scheschowitsch et al. 2017). TEER reflects the overall integrity of the endothelial barrier, which involves not only the expression of tight junction proteins, but also their optimal membrane localization, cytoskeletal anchoring, and interaction with other junctional proteins such as VE-cadherin (Vigh et al. 2021). These processes may require more robust or prolonged glucocorticoid receptor signalling, which is limited in HUVECs. Moreover, dexamethasone may also act through non-genomic or glucocorticoid receptor-independent pathways (Limbourg and Liao 2003), such as modulation of MAPK signalling or interaction with membrane-bound receptors (Yang and Zhang 2004). These pathways may be sufficient to modulate gene or protein expression, but not adequate to support full restoration endothelial barrier resistance as measured by TEER (Scheschowitsch et al. 2017).

Prior to protein synthesis during translation process, deoxyribonucleic acid (DNA) is transcribed into messenger ribonucleic acid (mRNA) in the nucleus in a process known as transcription (Sonenberg and Hinnebusch 2009). As expected, tHGA at 5 and 20 µM profoundly preserved the gene expression of ZO-1 and VE-cadherin during LPS induction based on RT-qPCR results. On the other hand, only 20 µM tHGA displayed a pronounced preservatory effect on occludin's gene expression. All these findings are in consistent with the results of Western Blotting, validating that tHGA preserved the gene expression of junctional proteins during the transcription process, which in turn preserved the downstream protein synthesis during the translation process. In overall, the findings of protein and gene

expression depict that, apart from inhibiting delocalization, tHGA was able to protect the endothelial barrier against LPS-induced hyperpermeability via the abolishment of junctional protein downregulation at transcriptional level.

Gene regulatory networks including gene expression are triggered by the activation of various signalling pathways when cells transform external stimuli. In LPS-induced endothelial hyperpermeability, both MyD88-dependent and -independent pathways are activated. In the MyD88-independent pathway, internalization and homodimerization of TLR4 occur upon the binding of LPS to the receptor complex TLR4, which then lead to the formation of complex with GEF-H1 (Salvador et al. 2016). Being a Rho-specific GEF, GEF-H1 acts as an upstream regulator which activates the member of Rho family of Rho GTPase, namely RhoA. Once RhoA is activated, it becomes a molecular switch which cycles from inactive GDP-bound state to active GTP-bound state. The resulting active RhoA-GTP subsequently triggers the activation of downstream effector ROCK, which in turn inhibits MLCP leading to MLC phosphorylation (Spindler et al. 2010). Consequently, phosphorylated MLC paves way to increased rearrangement of cortical F-actin into stress fiber with overwhelming actomyosin contractility (Komarova et al. 2017; Zhou et al. 2013). Chong et al. (2016) demonstrated that tHGA inhibited F-actin cytoskeletal rearrangement, thus attenuating stress fiber formation in the presence of LPS (Chong et al. 2016). The present study further demonstrates that tHGA exerted such effect by targeting MLC, the most downstream signalling molecule in the GEF-H1/RhoA/ROCK pathway. Inhibition of MLC phosphorylation by tHGA is thought to interrupt LPS-induced F-actin cytoskeletal rearrangement. Beside MLC, the present study also demonstrates that tHGA was able to significantly abolish the activation of NF-κB p65, p38 MAPK, and ERK MAPK signal transduction pathways during LPS induction, all of which are also downstream targets of ROCK (Guo et al. 2012). These findings may explain the abilities of tHGA to suppress ICAM-1 and VCAM-1 expression (Yan et al. 2002; Cho et al. 2014), PGE_2 overexpression (Mitsuhashi et al. 2004), monocyte adhesion (Jiang et al. 2013), and stress fiber formation (Qin et al. 2015), as well as junctional protein disruption (Mitsuhashi et al. 2004; Kevil et al. 2000; Xia et al. 2014). Surprisingly, tHGA failed to inhibit the phosphorylation of JNK MAPK in the presence of LPS. As JNK MAPK is not a signalling molecule in GEF-H1/RhoA/ROCK pathway, this result implies that the protective effects of tHGA on junctional proteins were primarily attributed to the inactivation of GEF-H1/RhoA/ROCK pathway, which in turn abrogated the activation of downstream signalling molecules including MLC, NF-κB p65, p38 MAPK, and ERK MAPK.

As the experimental findings firmly proved that protective effects of tHGA on junctional proteins were primarily attributed to the inactivation of GEF-H1/RhoA/ROCK pathway via MLC, molecular docking was employed to predict the molecular target of tHGA. ROCK is the upstream molecule of MLC which is implicated in various responses including ICAM-1 expression, and activation of p38 MAPK and ERK MAPK, as well as NF-κB translocation. The findings reveal that tHGA may directly bind to human ROCK1, and its ability to interact with key amino acid residues involved in stabilizing the protein-inhibitor complex may contribute to its efficacy. Therefore, ROCK1 could be the molecular target of tHGA underlying its junctional protective effects during LPS-induced endothelial hyperpermeability. However, it is recommended that ROCK1 kinase activity assay should be performed in the future to examine the mechanism of tHGA direct inhibition of ROCK1. The overall mechanisms and signalling pathways underlying the junctional protective effects of tHGA in LPS-induced endothelial hyperpermeability are summarized in Fig. 10.

A pharmacokinetics study using absorption, distribution, metabolism, elimination, and toxicity (ADMET) analysis revealed that tHGA exhibited good intestinal absorption, good aqueous solubility, and moderate blood–brain barrier penetration, with protein plasma binding ability and cytochrome P4502D6 (CYP2D6) inhibitory effect, and had no hepatotoxicity (Ng et al. 2018). Additionally, a toxicology study of tHGA via toxicity prediction by komputer-assisted technology (TOPKAT) further revealed that tHGA was biodegradable, non-mutagenic, non-carcinogenic, skin non-irritant, and ocular non-irritant, thus suggesting the potential safety of tHGA for therapeutic use (Ng et al. 2018). Interestingly, despite the oral bioavailability of tHGA is not high, it has been extensively proven to be very potent in numerous pre-clinical studies (Alkhateeb et al. 2020). Specifically, a pharmacodynamics study via in vitro enzymatic and cell-based assays demonstrated that tHGA was a potent dual LOX/COX inhibitor with higher selectivity towards 5-LOX (IC_{50} = 0.42 μM) and COX-2 (IC_{50} = 0.4 μM) (Shaari et al. 2011). Although tHGA was more selective towards 5-LOX, it was also found to be inhibitory against 15-LOX with IC_{50} of 23.6 μM, with an analogue showing significantly high inhibition (IC_{50} = 10.3 μM) (Ng et al. 2018). Nonetheless, it is recommended that tHGA should be encapsulated with liposome to improve its oral bioavailability and pharmacokinetic profile. This was evidenced by another pharmacokinetics study which reported a 2.3-fold increment in the oral bioavailability of tHGA through liposomal encapsulation (Alkhateeb et al. 2020).

Despite that the efficacy and safety of tHGA have not been tested in human subject, Eczefolia™, our patented acetophenone-rich MP standardized extract with tHGA as the key marker, has currently undergone human clinical trial (Patent

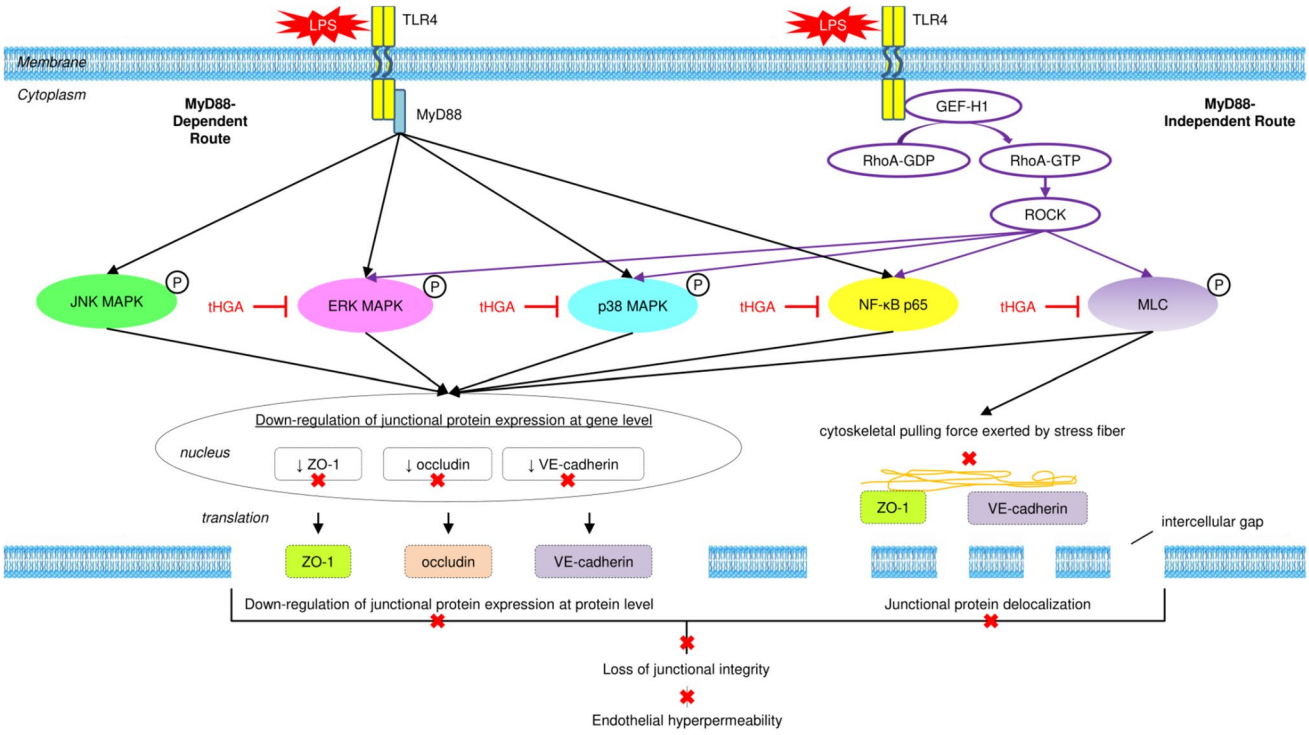

Fig. 10 Overall mechanisms and signalling pathways underlying the junctional protective effects of 2,4,6-trihydroxy-3-geranyl acetophenone (tHGA) in lipopolysaccharide (LPS)-induced endothelial hyperpermeability

title: A *Melicope Ptelefolia* Enriched Extract as Alternative for Eczema Treatment; Patent number: PI2024006146). Eczefolia™ has been proven to exhibit promising in vitro anti-allergic inflammatory and in vivo atopic dermatitis-mitigating effects (under review). The preliminary findings of our ongoing human clinical trial indicate that the daily intake of Eczefolia™ up to 200 mg was not only effective in managing the allergy symptoms, but also proven to be safe with no toxic sign and adverse reactions in 50 allergic patients tested. Although the effect of Eczefolia™ has not been investigated in endothelial hyperpermeability-related disorders, the prominent mast cell stabilizing effect of Eczefolia™ proven in allergy context is partly contributed by the inhibition of F-actin cytoskeletal rearrangement (important effect leading to attenuation of endothelial hyperpermeability), which consequently prevents the degranulation and secretion of mast cell mediators to the surrounding. Taken together, it is highly probable that tHGA, the major marker in Eczefolia™, is safe to be consumed and effective in treating endothelial hyperpermeability in human as well. Additionally, toxicology study of tHGA via TOPKAT further revealed that tHGA was biodegradable, non-mutagenic, non-carcinogenic, skin non-irritant, and ocular non-irritant (Ng et al. 2018). Despite that this is a computational modelling, the finding somehow strengthens the postulation mentioned above that tHGA is safe for consumption and not toxic in human subject.

Despite that our study has proven the significant protective effects of tHGA against junctional protein disruption during LPS-induced endothelial hyperpermeability, there are several limitations and recommendations for future research. The findings of molecular docking revealed that ROCK1 was the molecular target of tHGA during LPS induction, which was further validated by rescue experiment via TEER. As molecular docking is a prediction via computational modelling, it is recommended that further investigation using wet laboratory experiments such as ROCK1 kinase activity assay and gene transfection knockdown approach should be performed in the future to examine the mechanism of tHGA's direct inhibition on ROCK1. Moreover, although HUVECs have been commonly used to investigate endothelial hyperpermeability in vitro thus far (Medina-Leyte et al. 2020), it displays variations in biological characteristics as compared to other endothelial cell types, which render it slightly less experimentally representable. This is because HUVECs are derived from immune-naive foetal tissue which displays functional differences with adult vascular endothelium. Therefore, it is recommended that the protective effects of tHGA proven in the present study should be further validated using other endothelial cell types such as human saphenous vein endothelial cells (HSVECs) (Tan et al. 2004) and human lung microvascular endothelial cells (HMVEC-Ls) (Taniguchi et al. 2020).

Conclusions

In conclusion, tHGA exhibited significant protective effects against junctional protein disruption by inhibiting both localization and expression of ZO-1, occludin, and VE-cadherin in LPS-induced endothelial hyperpermeability. These effects were attributed to the inactivation of MLC, NF-κB p65, p38 MAPK, and ERK MAPK signalling molecules, which are mainly diverged from GEF-H1/RhoA/ROCK pathway under the MyD88-independent route. Further investigation via molecular docking predicts that ROCK1 could be the molecular target of tHGA underlying its junctional protective effects during LPS-induced endothelial hyperpermeability. As such, it is highly recommended that tHGA should be further developed into a potential therapeutic remedy for the prevention and/or treatment of various disorders related to uncontrolled or prolonged endothelial hyperpermeability.

Supplementary information The online version contains supplementary material available at https://doi.org/10.1007/s00210-025-04627-5.

Acknowledgements The authors would like to thank the members of Cell Signalling Lab, Faculty of Medicine and Health Sciences, Universiti Putra Malaysia (UPM), for providing technical supports for this study, as well as the Future Food Universiti-Driven Research Programme (UDRP) at UPM for their generous support. The authors also want to acknowledge Miss Elvia Ramawy and Miss Arisha Syeda Maqsood from Monash University Malaysia for their contributions in immunofluorescence staining and molecular docking, respectively.

Author contributions Conceptualization, funding acquisition and project administration: CLT and MM; Methodology, investigation, data curation and formal analysis: YHC, KYL and KR; Resources: KS; Supervision: HHH, JWT, DAI and CLT; Validation: HHH, JWT, DAI, KS and CLT; Visualization: YHC and CLT; Writing – original draft: YHC and KR; Writing – review: all authors. The authors declare that all data were generated in-house and that no paper mill was used.

Funding Open access funding provided by The Ministry of Higher Education Malaysia and Universiti Putra Malaysia. This study was funded by Ministry of Higher Education, Malaysia under Fundamental Research Grant Scheme [FRGS/1/2023/SKK15/UPM/02/3] and Universiti Malaysia Sabah under Skim Pensyarah Lantikan Baru [SLB2281]. YHC and KYL were the recipients of Graduate Research Fellowship (GRF) and Graduate Research Assistantship (GRA), respectively.

Data availability The data supporting the findings of this study are provided as supplementary materials. For the raw images of Western Blotting, the bands were labelled according to their respective experimental groups. N: normal control; V: vehicle control; tHGA: tHGA control; NC: negative control; 1.25: 1.25 μM tHGA pre-treatment + LPS; 5: 5 μM tHGA pre-treatment + LPS; 20: 20 μM tHGA pre-treatment + LPS; Dex: dexamethasone pre-treatment + LPS; Inh: tHGA pre-treatment + inhibitor + LPS. Moreover, the images of SDS-PAGE gel and membrane with visible protein ladder and their respective molecular weights are also provided in the supplementary material.

Declarations

Competing interests The authors declare no competing interests.

References

Alkhateeb Y, Jarrar QB, Abas F, Rukayadi Y, Tham CL, Hay YK, Shaari K (2020) Pharmacokinetics and metabolism of liposome-encapsulated 2,4,6-trihydroxygeranylacetophenone in rats using high-resolution orbitrap liquid chromatography mass spectrometry. Molecules 25(13):3069. https://doi.org/10.3390/molecules25133069

Basuroy S, Sheth P, Kuppuswamy D, Balasubramanian S, Ray RM, Rao, RK (2003) Expression of kinase-inactive c-Src delays oxidative stress-induced disassembly and accelerates calcium-mediated reassembly of tight junctions in the Caco-2 cell monolayer. J Biol Chem 278(14):11916–11924

Beroza P, Crawford JJ, Ganichkin O, Gendelev L, Harris SF, Klein R, Miu A, Steinbacher S, Klingler FM, Lemmen C (2022) Chemical space docking enables large-scale structure-based virtual screening to discover ROCK1 kinase inhibitors. Nat Comm 13:6447–6456. https://doi.org/10.1038/s41467-022-33981-8

Chan YH, Harith HH, Israf DA, Tham CL (2020) Differential regulation of LPS-mediated VE-cadherin disruption in human endothelial cells and the underlying signaling pathways: a mini review. Front Cell Dev Biol 7:280–289. https://doi.org/10.3389/fcell.2019.00280

Chan YH, Musa NF, Chong YJ, Saat SA, Hafiz F, Shaari K, Israf DA, Tham CL (2021) 2, 4, 6-trihydroxy-3-geranyl acetophenone suppresses vascular leakage and leukocyte infiltration in lipopolysaccharide-induced endotoxemic mice. Pharm Biol 59:732–740. https://doi.org/10.1080/13880209.2021.1933083

Cho YS, Kim CH, Kim HN, Ha TS, Ahn HY (2014) Ginsenoside Rg3 inhibits lipopolysaccharide–induced adhesion molecule expression in human umbilical vein endothelial cell and C57BL/6 mice. Die Pharmazie-an Int J Pharm Sci 69:818–822. https://doi.org/10.1691/ph.2014.4611

Chong YJ, Musa NF, Ng CH, Shaari K, Israf DA, Tham CL (2016) Barrier protective effects of 2, 4, 6-trihydroxy-3-geranyl acetophenone on lipopolysaccharides-stimulated inflammatory responses in human umbilical vein endothelial cells. J Ethnopharmacol 192:248–255. https://doi.org/10.1016/j.jep.2016.07.032

Claesson-Welsh L, Dejana E, McDonald DM (2020) Permeability of the endothelial barrier: identifying and reconciling controversies.

Trends Mol Med 27:314–331. https://doi.org/10.1016/J.MOLMED.2020.11.006
Daiber A, Steven S, Weber A, Shuvaev VV, Muzykantov VR, Laher I, Li H, Lamas S, Münzel T (2017) Targeting vascular (endothelial) dysfunction. Br J Pharmacol 174:1591–1619. https://doi.org/10.1111/bph.13517
Dolmatova EV, Wang K, Mandavilli R, Griendling KK (2021) The effects of sepsis on endothelium and clinical implications. Cardiovasc Res 117:60–73. https://doi.org/10.1093/CVR/CVAA070
Dorland YL, Huveneers S (2017) Cell–cell junctional mechanotransduction in endothelial remodeling. Cell Mol Life Sci 74:279–292. https://doi.org/10.1007/S00018-016-2325-8
Dudek SM, Garcia JG (2001) Cytoskeletal regulation of pulmonary vascular permeability. J Appl Physiol 91:1487–1500. https://doi.org/10.1152/jappl.2001.91.4.1487
Evoy KE, Abel SR (2013) Ranibizumab: the first vascular endothelial growth factor inhibitor approved for the treatment of diabetic macular edema. Ann Pharmacother 47(6):811–818
Fakir S, Barabutis N (2024) Involvement of ATF6 in octreotide-induced endothelial barrier enhancement. Pharmaceuticals 17(12):1604
Fakir S, Kubra KT, Barabutis N (2024) Octreotide protects against LPS-induced endothelial cell and lung injury. Cell Signal 124:111455
Garrett JP, Lowery AM, Adam AP, Kowalczyk AP, Vincent PA (2017) Regulation of endothelial barrier function by p120-catenin• VE-cadherin interaction. Mol Biol Cell 28:85–97. https://doi.org/10.1091/MBC.E16-08-0616
Gomes-Porras M, Cárdenas-Salas J, Álvarez-Escolá C (2020) Somatostatin analogs in clinical practice: a review. Int J Mol Sci 21(5):1682
Guo F, Zhou Z, Dou Y, Tang J, Gao C, Huan J (2012) Gef-h1/rhoa signalling pathway mediates lipopolysaccharide-induced intercellular adhesion molecular-1 expression in endothelial cells via activation of p38 and NF-κb. Cytokine 57:417–428. https://doi.org/10.1038/ijos.2017.51
Guo W, Wang P, Liu ZH, Ye P (2018) Analysis of differential expression of tight junction proteins in cultured oral epithelial cells altered by *Porphyromonas gingivalis*, *Porphyromonas gingivalis* lipopolysaccharide, and extracellular adenosine triphosphate. Int J Oral Sci 10(1):1–7
Hu D, Yang X, Xiang Y, Li H, Yan H, Zhou J, Caudle Y, Zhang X, Yin D (2015) Inhibition of toll-like receptor 9 attenuates sepsis-induced mortality through suppressing excessive inflammatory response. Cell Immunol 295:92–98
Huang SY, Zou X (2010) Advances and challenges in protein-ligand docking. Int J Mol Sci 11:3016–3034. https://doi.org/10.3390/ijms11083016
Huang Y, Tan Q, Chen R, Cao B, Li W (2015) Sevoflurane prevents lipopolysaccharide-induced barrier dysfunction in human lung microvascular endothelial cells: Rho-mediated alterations of VE-cadherin. Biochem Biophys Res Commun 468:119–124. https://doi.org/10.1016/j.bbrc.2015.10.150
Ismail N, Jambari NN, Zareen S, Akhtar MN, Shaari K, Zamri-Saad M, Tham CL, Sulaiman MR, Lajis NH, Israf DA (2012) A geranyl acetophenone targeting cysteinyl leukotriene synthesis prevents allergic airway inflammation in ovalbumin-sensitized mice. Toxicol Appl Pharmacol 259:257–262. https://doi.org/10.1016/j.taap.2012.01.003
Jacobs M, Hayakawa K, Swenson L, Bellon S, Fleming M, Taslimi P, Doran J (2006) The structure of dimeric ROCK I reveals the mechanism for ligand selectivity. J Biol Chem 281:260–268. https://doi.org/10.1074/jbc.M508847200
Jiang SJ, Hsu SY, Deng CR, Huang HC, Liu SL, Shi GY, Wu HL (2013) Dextromethorphan attenuates LPS-induced adhesion molecule expression in human endothelial cells. Microcirculation 20:190–201. https://doi.org/10.1111/micc.12024
Kale G, Naren AP, Sheth P, Rao RK (2003) Tyrosine phosphorylation of occludin attenuates its interactions with ZO-1, ZO-2, and ZO-3. Biochem Biophys Res Commun 302:324–329. https://doi.org/10.1016/S0006-291X(03)00167-0
Karim AM, Nasouddin SS, Othman M, Mohd Adzahan N, Hussin SR (2011) Consumers' knowledge and perception towards *Melicope ptelefolia* (daun tenggek burung): a preliminary qualitative study. Int Food Res J 18:1481
Kevil CG, Oshima T, Alexander B, Coe LL, Alexander JS (2000) H_2O_2-mediated permeability: role of MAPK and occludin. Am J Physiol Cell Physiol 279(1):21–30. https://doi.org/10.1152/AJPCELL.2000.279.1.C21
Komarova YA, Kruse K, Mehta D, Malik AB (2017) Protein interactions at endothelial junctions and signaling mechanisms regulating endothelial permeability. Circ Res 120:179–206. https://doi.org/10.1161/CIRCRESAHA.116.306534
Lammer NC, Ashraf HM, Ugay DA, Spencer SL, Allen MA, Batey RT, Wuttke DS (2023) RNA binding by the glucocorticoid receptor attenuates dexamethasone-induced gene activation. Sci Rep 13(1):9385
Li H, Liu J, Zhang S, Luo T, Wu F, Dong J, Guo Y, Zhao L (2017) Corilagin ameliorates the extreme inflammatory status in sepsis through TLR4 signaling pathways. BMC Complement Med Ther 17(18):1–8. https://doi.org/10.1186/s12906-016-1533-y
Limbourg FP, Liao JK (2003) Nontranscriptional actions of the glucocorticoid receptor. J Mol Med 81(3):168–174
Liu H, Yu X, Yu S, Kou J (2015) Molecular mechanisms in lipopolysaccharide-induced pulmonary endothelial barrier dysfunction. Int Immunopharmacol 29:937–946. https://doi.org/10.1016/j.intimp.2015.10.010
Lowe J, Araujo J, Yang J, Reich M, Oldendorp A, Shiu V, Quarmby V, Lowman H, Lien S, Gaudreault J, Maia M (2007) Ranibizumab inhibits multiple forms of biologically active vascular endothelial growth factor in vitro and in vivo. Exp Eye Res 85(4):425–430
Löwenberg M, Stahn C, Hommes DW, Buttgereit F (2008) Novel insights into mechanisms of glucocorticoid action and the development of new glucocorticoid receptor ligands. Steroids 73(9–10):1025–1029
Medina-Leyte DJ, Domínguez-Pérez M, Mercado I, Villarreal-Molina MT, Jacobo-Albavera L (2020) Use of human umbilical vein endothelial cells (HUVEC) as a model to study cardiovascular disease: a review. Appl Sci 10(3):938. https://doi.org/10.3390/APP10030938
Mitsuhashi M, Liu J, Cao S, Shi X, Ma X (2004) Regulation of interleukin-12 gene expression and its anti-tumor activities by prostaglandin E2 derived from mammary carcinomas. J Leukoc Biol 76(2):322–332
Ng CH, Rullah K, Aba F, Lam KW, Ismail IS, Jamaludin F, Shaari K (2018) Hits-to-lead optimization of the natural compound 2,4,6-trihydroxy-3-geranyl-acetophenone (tHGA) as a potent LOX inhibitor: synthesis, structure-activity relationship (SAR) sStudy, and computational assignment. Molecules 23(10):2509. https://doi.org/10.3390/molecules23102509
Oray M, Abu Samra K, Ebrahimiadib N, Meese H, Foster CS (2016) Long-term side effects of glucocorticoids. Expert Opin Drug Saf 15(4):457–465
Pereira-Leite C, Nunes C, Jamal SK, Cuccovia IM, Reis S (2017) Non-steroidal anti-inflammatory therapy: a journey toward safety. Med Res Rev 37:802–859. https://doi.org/10.1002/med.21424

Pettersen EF, Goddard TD, Huang CC, Couch GS, Greenblatt DM, Meng EC, Ferrin TE (2004) UCSF chimera - a visualization system for exploratory research and analysis. J Comput Chem 25:1605–1612. https://doi.org/10.1002/jcc.20084

Pierce AC, Sandretto KL, Bemis GW (2002) Kinase inhibitors and the case for CH…O hydrogen bonds in protein-ligand binding. Proteins Struct Funct Bioinform 49:567–576. https://doi.org/10.1002/prot.10259

Prasain N, Stevens T (2009) The actin cytoskeleton in endothelial cell phenotypes. Microvasc Res 77:53–63. https://doi.org/10.1016/J.MVR.2008.09.012

Qin L, Huang W, Mo X, Chen Y, Wu X (2015) LPS induces occludin dysregulation in cerebral microvascular endothelial cells via MAPK signaling and augmenting MMP-2 levels. Oxid Med Cell Longev 120641:1–9. https://doi.org/10.1155/2015/120641

Rao R (2009) Occludin phosphorylation in regulation of epithelial tight junctions. Ann N Y Acad Sci 1165:62. https://doi.org/10.1111/J.1749-6632.2009.04054.X

Rullah K, Roney M, Ibrahim Z, Shamsudin NF, Islami D, Ahmed QU, Wai LK, Aluwi MFFM (2022) Identification of novel 5-lipoxygenase-activating protein (FLAP) inhibitors by an integrated method of pharmacophore virtual screening, docking, QSAR and ADMET analyses. J Comput Biophys Chem 22(1):1–21. https://doi.org/10.1142/S2737416523500059

Salvador B, Arranz A, Francisco S, Cordoba L, Punzon C, Llamas MÁ, Fresno M (2016) Modulation of endothelial function by toll like receptors. Pharmacol Res 108:46–56. https://doi.org/10.1016/J.PHRS.2016.03.038

Scheschowitsch K, Leite JA, Assreuy J (2017) New insights in glucocorticoid receptor signaling—more than just a ligand-binding receptor. Front Endocrinol 8:16

Schnoor M, Ponce AG, Vadillo E, Pelayo R, Rossaint J, Zarbock A (2017) Actin dynamics in the regulation of endothelial barrier functions and neutrophil recruitment during endotoxemia and sepsis. Cell Mol Life Sci 74:1985–1997. https://doi.org/10.1007/S00018-016-2449-X

Seth A, Sheth P, Elias BC, Rao R (2007) Protein phosphatases 2A and 1 interact with occludin and negatively regulate the assembly of tight junctions in the CACO-2 cell monolayer. J Biol Chem 282:11487–11498. https://doi.org/10.1074/JBC.M610597200

Shaari K, Suppaiah V, Wai LK, Stanslas J, Tejo BA, Israf DA, Abas F, Ismail IS, Shuib NH, Zareen S, Lajis NH (2011) Bioassay-guided identification of an anti-inflammatory prenylated acylphloroglucinol from *Melicope ptelefolia* and molecular insights into its interaction with 5-lipoxygenase. Bioorg Med Chem 19(21):6340–6347. https://doi.org/10.1016/j.bmc.2011.09.001

Shen M, Tian S, Pan P, Sun H, Li D, Li Y, Zhou H, Li C, Lee SMY, Hou T (2015) Discovery of novel ROCK1 inhibitors via integrated virtual screening strategy and bioassays. Sci Rep 5(16749):1–14. https://doi.org/10.1038/srep16749

Sonenberg N, Hinnebusch AG (2009) Regulation of translation initiation in eukaryotes: mechanisms and biological targets. Cell 136:731–745. https://doi.org/10.1016/J.CELL.2009.01.042

Spindler V, Schlegel N, Waschke J (2010) Role of GTPases in control of microvascular permeability. Cardiovasc Res 87:243–253. https://doi.org/10.1093/cvr/cvq086

Stahn C, Löwenberg M, Hommes DW, Buttgereit F (2007) Molecular mechanisms of glucocorticoid action and selective glucocorticoid receptor agonists. Mol Cell Endocrinol 275:71–78. https://doi.org/10.1016/j.mce.2007.05.019

Sullivan JT, Bulman CA, Salamat Z (2011) Effect of crude lipopolysaccharide from *Escherichia coli* O127: B8 on the amebocyte-producing organ of *Biomphalaria glabrata* (Mollusca). Dev Comp Immunol 35:1182–1185. https://doi.org/10.1016/J.DCI.2011.03.032

Tan PH, Chan C, Xue SA, Dong R, Ananthesayanan B, Manunta M, Kerouedan C, Cheshire NJW, Wolfe JH, Haskard DO, George AJT (2004) Phenotypic and functional differences between human saphenous vein (HSVEC) and umbilical vein (HUVEC) endothelial cells. Atherosclerosis 173(2):171–183. https://doi.org/10.1016/J.ATHEROSCLEROSIS.2003.12.011

Taniguchi D, Matsumoto K, Machino R, Takeoka Y, Elgalad A, Taura Y, Oyama S, Tetsuo T, Moriyama M, Takagi K, Kunizaki M, Tsuchiya T, Miyazaki T, Hatachi G, Matsuo N, Nakayama K, Nagayasu T (2020) Human lung microvascular endothelial cells as potential alternatives to human umbilical vein endothelial cells in bio-3d-printed trachea-like structures. Tissue Cell 63:101321. https://doi.org/10.1016/J.TICE.2019.101321

Tham CL, Liew CY, Lam KW, Mohamad AS, Kim MK, Cheah YK, Zakaria ZA, Sulaiman MR, Lajis NH, Israf DA (2010) A synthetic curcuminoid derivative inhibits nitric oxide and proinflammatory cytokine synthesis. Eur J Pharmacol 628(1–3):247–254. https://doi.org/10.1016/J.EJPHAR.2009.11.053

van der Wijk AE, Canning P, van Heijningen RP, Vogels IM, van Noorden CJ, Klaassen I, Schlingemann RO (2019) Glucocorticoids exert differential effects on the endothelium in an in vitro model of the blood–retinal barrier. Acta Ophthalmol 97(2):214–224

Vermette D, Hu P, Canarie MF, Funaro M, Glover J, Pierce RW (2018) Tight junction structure, function, and assessment in the critically ill: a systematic review. Intensive Care Med Exp 6(1):1–18. https://doi.org/10.1186/S40635-018-0203-4

Vestweber D, Wessel F, Nottebaum AF (2014) Similarities and differences in the regulation of leukocyte extravasation and vascular permeability. Semin Immunopathol 36:177–192. https://doi.org/10.1007/S00281-014-0419-7

Vigh JP, Kincses A, Ozgür B, Walter FR, Santa-Maria AR, Valkai S, Vastag M, Neuhaus W, Brodin B, Dér A, Deli MA (2021) Transendothelial electrical resistance measurement across the blood–brain barrier: a critical review of methods. Micromachines 12:685. https://doi.org/10.3390/mi12060685

Wang R, Lai L, Wang S (2002) Further development and validation of empirical scoring functions for structure-based binding affinity prediction. J Comput Aided Mol Des 16:11–26. https://doi.org/10.1023/A:1016357811882

Wang XY, Chen XL, Wang L, Chen HW (2015) High-dose glucocorticoids increases the expression of mineralocorticoid receptor in vascular endothelial cells. Eur Rev Med Pharmacol Sci 19(22)

Wu G, Robertson DH, Brooks CL III, Vieth M (2003) Detailed analysis of grid-based molecular docking: a case study of CDOCKER - a CHARMm-based MD docking algorithm. J Comput Chem 24:1549–1562. https://doi.org/10.1002/jcc.10306

Wu J, Deng Z, Sun M, Zhang W, Yang Y, Zeng Z, Wu J, Zhang Q, Liu Y, Chen Z, Guo X, Zhao K, Huang Q, Chen Z (2020) Polydatin protects against lipopolysaccharide-induced endothelial barrier disruption via SIRT3 activation. Lab Invest 100(4):643–656. https://doi.org/10.1038/s41374-019-0332-8

Xia JL, Wang LQ, Wu LL, Huang QB (2014) Doxycycline hyclate protects lipopolysaccharide-induced endothelial barrier dysfunction by inhibiting the activation of p38 mitogen-activated protein kinase. Biol Pharm Bull 37:1882–1890. https://doi.org/10.1248/bpb.b14-00298

Yan W, Zhao K, Jiang Y, Huang Q, Wang J, Kan W, Wang S (2002) Role of p38 MAPK in ICAM-1 expression of vascular endothelial

cells induced by lipopolysaccharide. Shock 17:433–438. https://doi.org/10.1097/00024382-200205000-00016
Yang S, Zhang L (2004) Glucocorticoids and vascular reactivity. Curr Vasc Pharmacol 2(1):1–12
Yang J, Yao W, Qian G, Wei Z, Wu G, Wang G (2015) Rab5-mediated VE-cadherin internalization regulates the barrier function of the lung microvascular endothelium. Cell Mol Life Sci 72:4849–4866. https://doi.org/10.1007/s00018-015-1973-4
Yu CX, Tan JW, Rullah K, Imran S, Tham CL (2023) Insight parameter drug design for human β-tryptase inhibition integrated molecular docking, QSAR, molecular dynamics simulation, and pharmacophore modelling studies of α-keto-[1, 2, 4]-oxadiazoles. J Biomol Struct Dyn 41:12978–12996. https://doi.org/10.1080/07391102.2023.2171131
Zhou Z, Guo F, Dou Y, Tang J, Huan J (2013) Guanine nucleotide exchange factor-H1 signaling is involved in lipopolysaccharide-induced endothelial barrier dysfunction. Surgery 154:621–631. https://doi.org/10.1016/j.surg.2013.04.009

Authors and Affiliations

Yee Han Chan[1] · Kong Yen Liew[1] · Kamal Rullah[2] · Hanis Hazeera Harith[1] · Ji Wei Tan[3] · Daud Ahmad Israf[1] · Khozirah Shaari[4,5] · Mexmollen Marcus[6] · Chau Ling Tham[1]

✉ Mexmollen Marcus
mex.marcus@ums.edu.my

✉ Chau Ling Tham
chauling@upm.edu.my

Yee Han Chan
yeehan1995@hotmail.com

Kong Yen Liew
kongyen0531@gmail.com

Kamal Rullah
kamalrullah@iium.edu.my

Hanis Hazeera Harith
hanishazeera@upm.edu.my

Ji Wei Tan
tan.jiwei@monash.edu

Daud Ahmad Israf
daudaia@upm.edu.my

Khozirah Shaari
khozirah@upm.edu.my

1 Department of Biomedical Sciences, Faculty of Medicine and Health Sciences, Universiti Putra Malaysia, Serdang 43400, Selangor, Malaysia

2 Department of Pharmaceutical Chemistry, Kulliyyah of Pharmacy, International Islamic University Malaysia, Bandar Indera Mahkota, Kuantan 25200, Pahang, Malaysia

3 School of Science, Monash Universiti Malaysia, Subang Jaya 47500, Selangor, Malaysia

4 Natural Medicine and Product Research Laboratory, Institute of Bioscience, Universiti Putra Malaysia, Serdang 43400, Selangor, Malaysia

5 Department of Chemistry, Faculty of Science, Universiti Putra Malaysia, Serdang 43400, Selangor, Malaysia

6 Department of Emergency Medicine, Faculty of Medicine and Health Sciences, Universiti Malaysia Sabah, Kota Kinabalu 88400, Sabah, Malaysia